
Article:

Charoenwong, C, Connolly, DP, Woodward, PK et al. (2022) Analytical forecasting of long-term railway track settlement. Computers and Geotechnics, 143. 104601. ISSN: 0266-352X

https://doi.org/10.1016/j.compgeo.2021.104601

Title: Analytical forecasting of long-term railway track settlement

C. Charoenwong[a], D.P. Connolly[a,*], P.K. Woodward[a], P. Galvín[b, c], P. Alves Costa[d]

[a] *Institute for High Speed Rail and Systems Integration, School of Civil Engineering, University of Leeds, UK*

[b] *Escuela Técnica Superior de Ingeniería, Universidad de Sevilla, Camino de los Descubrimientos s/n, 41092, Sevilla, Spain*

[c] *Laboratory of Engineering for Energy and Environmental Sustainability, Universidad de Sevilla, Camino de los Descubrimientos s/n, 41092, Sevilla, Spain*

[d] *Faculty of Engineering, University of Porto, Portugal*

Keywords:

Railway track geometry; Ballast settlement modelling; Subgrade settlement modelling; Railway track-ground settlement; Vehicle-track interaction; Railway track-ground non-linearity

Abstract

Railway tracks undergo plastic settlement when subject to repeated train loading. This occurs differentially along the track rather than in a uniform manner, and the profile is a key parameter when scheduling track maintenance operations. Therefore this paper presents a novel numerical approach to predict track irregularity evolution. The model combines empirical settlement laws with finite element theory, where the track-ground structure is modelled explicitly, and multi-body train-track interaction is considered. The stresses induced by rolling stock are solved using a hybrid frequency-wavenumber and time-space approach, considering non-linear track-soil material behaviour. It has several novelties: 1) after every load passage, the track profile is updated before applying the next load, meaning the train-track interaction is constantly evolving; 2) new empirical settlement laws are derived that account for evolving train-track forces and track profiles; 3) fully 3D stress fields in the track and ground are considered. First the model is described, before validating its prediction of track geometry evolution, captured from track recording vehicles. Next, it's used to show that modelling error is introduced if the geometry isn't updated frequently (e.g. after every load passage). Finally, a parametric study shows track subgrade material properties have a marked effect on track settlement.

1. Introduction

Under every axle passage, railway tracks experience a small amount of permanent deformation (Li et al., 2015). Due to dynamic loading and varying track support conditions along the track, successive axle passage lead to long-term non-uninform (aka differential) settlement (Fröhling, 1998). These changes in track level over a given distance define the track geometry. Track geometry can deteriorate rapidly once differential settlement starts to occur, because degradation induces higher train-track dynamic interaction forces, thus leading to further track settlement.

Track quality measurement is typically performed by a track recording car and a variety of metrics can be used to define a track quality index (TQI) (Yan and Corman, 2020). Different countries have developed and implemented TQI's in different ways, however, the standard deviation (SD) of vertical track geometry over a given distance is widely used (Neuhold et al., 2020). The higher the SD value, the lower quality of the track. When the SD of the track geometry reaches a threshold limit value, maintenance action is required.

Tamping is a common track maintenance activity used to correct vertical track geometry faults for wavelengths within a certain range (for example, between 3-25 m (Esveld, 2001), or 3-35m (Network Rail, 2015)). When the variation in geometry exceeds a threshold limit, corrective tamping restores it to an acceptable value, thus helping to extend the track life between full track reconstructions. Rather than wait until a SD threshold value is reached and then perform emergency maintenance, common practise is to attempt to predict the future date when maintenance is required. Then it can be planned, resulting in minimal line disruption. To predict these maintenance schedule dates, most commonly, on existing lines, historical changes in track geometry at a given location are extrapolated into the future to determine degradation (Lee et al., 2020). However, this approach is challenging for cases where significant changes are made to the track or rolling stock. In such situations, historical data is unlikely to be representative of future behaviour. For example:

- New track construction. In this case historical geometry records don't exist.
- The changing of rolling stock characteristics. For example, raising line speed, increased freight-passenger traffic ratios, and deploying new rolling stock. In these cases, the changes in vehicle-track dynamics will lead to different dynamic stress fields in the track. Therefore the settlement rate may be different from historical.
- The changing of track characteristics. For example, new track designs, adding new track components, and renewing the track/subgrade. In these cases the dynamic stiffness and strength characteristics of the track may lead to settlement rates that differ from historical.

There are two main modelling approaches to predict track settlement: constitutive and empirical. Models based on constitutive relationships attempt to simulate the physical behaviour of materials, using for example, yield criterions, flow rules and hardening rules (Dahlberg, 2001; Indraratna et al., 2012; Suiker and de Borst, 2003). These can be implemented within a finite element model, however the discrete element method (DEM) can also be used to simulate local deformations and heterogeneous particle displacements (Guo et al., 2020; Saussine et al., 2006). Considering the FE approach, an implementation in 3D made in a commercial FE software combining with an elasto-plastic constitutive model was presented by (Shih et al., 2019) to calculate differential settlement in ballasted tracks. A constitutive model integrated with an iterative procedure was developed in (Li et al., 2016) to compute differential track settlement accounting for longitudinal variations in load and track characteristics. However, a challenge with such constitutive models is that they often require input parameters related to the ballast and subgrade that are difficult to measure/quantify. Further, they are often computationally intensive, thus making the prediction of long-term differential settlement due to dynamic train loads challenging (Chen and McDowell, 2016; Shan et al., 2017).

An alternative approach for settlement modelling is to use empirical settlement equations. Several models, see for example (Indraratna and Nimbalkar, 2013; ORE, 1970; Sato, 1995; Shenton, 1985), have been developed for the prediction of ballast settlement under cyclic loading. These typically identify empirical parameters using cyclic triaxial test data, reduced-scale models (Menan Hasnayn et al., 2017; Yu et al., 2019), or in situ measurements. Similarly, empirical parameters for the prediction of subgrade settlement have been obtained by conducting laboratory tests on different soil conditions to investigate plastic deformation under repeated load applications (Li, 1994; Li and Selig, 1996; Liu and Xiao, 2010). Compared with constitutive modelling, the published results achieved using empirical models are similar in accuracy to constitutive ones, however only depend upon a minimal number of input parameters that are usually relatively straightforward to determine (Ramos et al., 2020).

However, one drawback of the existing empirical models presented in the literature is that they assume the ballast and subgrade materials are subject to cyclic loads of equivalent magnitudes. This is not the case in real life, because track irregularities evolve with each axle passage. Therefore, for each subsequent passage, the train-track dynamic interaction forces, the distribution of stresses within the track layers, and ultimately the induced settlement is different. Further, in real life, most tracks are subject to mixed types of rolling stock (e.g. freight and passenger), running together on a timetable. In such situations, where the simulation of multiple vehicles is required, it is challenging to use the current forms of empirical settlement equations, because the dynamic loads are different for each vehicle.

A key input to constitutive and empirical settlement models are stresses induced in both ballast and subgrade. These stresses are often calculated using a numerical mode. One example of using numerical modelling combined with empirical settlement laws is presented by Sayeed and Shahin (Sayeed and Shahin, 2018). Settlement is calculated in both the ballast and subgrade, using a 3D finite element approach to compute the deviatoric stress, considering the effect of a moving dynamic train load. However, the track geometry profile is not updated after subsequent axle passages. Instead an empirical settlement law is used to extrapolate its change, based upon the results of the initial train passage. This is a drawback because changes in the track geometry influence the train-track interaction forces, which are closely linked to track unevenness (Burrow et al., 2017). Therefore, under certain circumstances, this approach may under-predict the deterioration of track geometry.

Alternatively, methodologies have been proposed to predict differential track settlement considering train-track dynamic interaction, accounting for the evolution of track geometry irregularities. For example, Zuada Coelho (Zuada Coelho et al., 2021) introduces a methodology to predict track settlement considering the effect of traffic changes, but at the network scale. The corresponding forces due to the dynamic deformation during train operation are computed, however not every axle passage is considered. Alternatively, Guo and Zhai (Guo and Zhai, 2018) apply an iterative method to estimate the long-term settlement of ballastless track, considering the evolution of differential settlement in the subgrade. An empirical model for subgrade settlement is proposed. The deviatoric stress exerted on the surface of subgrade is combined with an exponential attenuation equation. Further, Nielsen and Li (Nielsen and Li, 2018) propose a numerical method based on an iterative approach combined with an empirical model to predict the deterioration of track geometry due to differential settlement. The foundation is modelled using a beam-on-elastic-foundation approach (i.e. springs and dampers). Grossoni (Grossoni et al., 2021) presents a semi-analytical approach based on an investigation of material behaviour under cyclic loading combined with a train-track interaction model, that allows for the estimation of differential ballast settlement due to evolving track roughness. Plastic settlement is modelled at each loading cycle as a function of the vertical stress.

A common strategy in the aforementioned approaches is to model the track using springs and dashpots, and then solve in the time domain. Although this provides some advantages, it doesn't allow for the calculation of 3D dynamic stress fields in the track and the subgrade. Deviatoric stress is one of the most influential parameters on permanent deformation (Indraratna et al., 2010; Li and Selig, 1996) and therefore is closely linked to differential settlement. Although deviatoric stresses can be calculated in 2D, which is acceptable for certain engineering applications, when considering wave propagation problems, 3D modelling provides highest accuracy (Arcos et al., 2021; Xu et al., 2015). Therefore for railway applications that require accurate stress wave simulation (e.g. ground-borne vibration and critical velocity) the calculation of 3D fields has become standard practise.

In an attempt to address these challenges, this paper first proposes several recommended characteristics to calculate differential railway track settlements. Then a practical implementation of these characteristics is shown by developing a novel numerical approach capable of considering 3D stress fields, evolving track geometry and train-track interaction forces. The model is based on a FEM-PML (Finite Element Method with Perfectly Matched Layers) approach, solved in a hybrid manner, across both frequency-wavenumber and time-space domains. Train-track interaction, vehicle dynamics and 3D stress field propagation are modelled explicitly. After every load passage, the vertical track irregularities along the track length are updated, and the train-track dynamic interaction force and the distribution of dynamic stress are recalculated as a consequence. By taking advantage of a mixed frequency-wavenumber, time-space domain approach, the computational efficiency of the implementation is high, and thus allows the differential settlement to be updated after every train axle passage, even when using solid elements to capture 3D stress fields. Further, to maximise accuracy for heavy and fast moving axle loads, the non-linear stiffness characteristics of both the granular track and subgrade materials are accounted for.

2. Characteristics of a differential settlement prediction model

Long-term track geometry changes are important for predicting future maintenance schedules, particularly automated tamping. Therefore any numerical model should be able to predict differential settlement for the wavelength range over which tamping is effective, and the timeline until the next tamping cycle should be scheduled. The forecasting of long-term track settlement is challenging, involving numerous variables such as train-track interaction, an evolving track profile and non-linear soil behaviour. Further, when considering a large number of load passages, small inaccuracies at each iteration are magnified and can greatly affect the final predicted settlement. Thus, for a numerical approach attempting to do this, the following are important to consider:

1. Calculation of 3D stress fields in the track and ground. This is important because deviatoric stress is an influential parameter on settlement

2. Calculation of train-track interaction forces. The dynamic forces caused by the interaction between track geometry irregularities and rolling stock are a key source of differential settlement on plain line. The degradation of track geometry results in higher train-track dynamic interaction forces which effect on the distribution of the stresses, and thus further track settlement (Bian et al., 2015).

3. Simulation of the evolution of train-track interaction forces. Track geometry degrades after train passages, meaning future train passages are likely to generate different deviatoric stresses and differential settlement, compared to previous trains. This is particularly important when modelling a line with mixed rolling stock.

4. Simulation of the evolution of track-subgrade settlement laws. Track settlement rate is dependent upon the settlements from ballast and subgrade layers induced by previous axle loads. Considering the dynamic forces exerted on the track change as the track geometry evolves, the settlement relationship should consider this.

These characteristics can be achieved using different modelling approaches. For example, a direct approach can be used where non-linear soil behaviour is modelled directly. Alternatively, an indirect approach can be used, where the ground stress fields are estimated using an equivalent linear approach, and then the stress fields used to compute settlement using empirical laws. Although the first approach is more exact from the theoretical viewpoint, its application requires significant computational resources and the estimation of many input parameters to accurately define non-linear soil behaviour. Therefore, with the aim of acting as a practical tool for engineering purposes, the second strategy is preferred.

3. Numerical modelling overview

A variety of numerical simulation approaches can be used to meet the characteristics mentioned above, however the criteria imply that the problem should be modelled in 3D, consider vehicle dynamics and train-track interaction, and be able to update the track geometry after an arbitrary number of loads with arbitrary magnitude. To achieve these objectives, this paper proposes a novel, 2-step coupled modelling strategy, solved in a hybrid manner, across both time-space and frequency-wavenumber domains. The two primary steps are as shown in Figure 1:

Step A: Calculates the 3D elastodynamic response of the track-ground system in the frequency-wavenumber domain. The geo-static stresses and the moving load transfer function that accounts for soil stiffness non-linearity are computed. The 3D stress fields, which include quasi-static and dynamic components, are then calculated in terms of wavenumber and frequency. This part is only computed once for each moving speed of vehicle being considered. Also, the matrices for train and track compliance required for train-track dynamic interaction are computed. These various pre-calculated fields then allow Step B to be computed in an efficient manner for every axle passage.

Step B: Calculates the differential track settlement using a combination of time and frequency domain methods. The train-track dynamic interaction force, the deviator stress and the settlement in the track and ground are calculated. The total deviator stress includes quasi-static stress, dynamic stress and geo-static stress. After every load passage the track irregularity profile is updated and thus the new train-track dynamic force is recalculated.

These steps are repeated until the defined number of load cycles or threshold geometry criteria is reached.

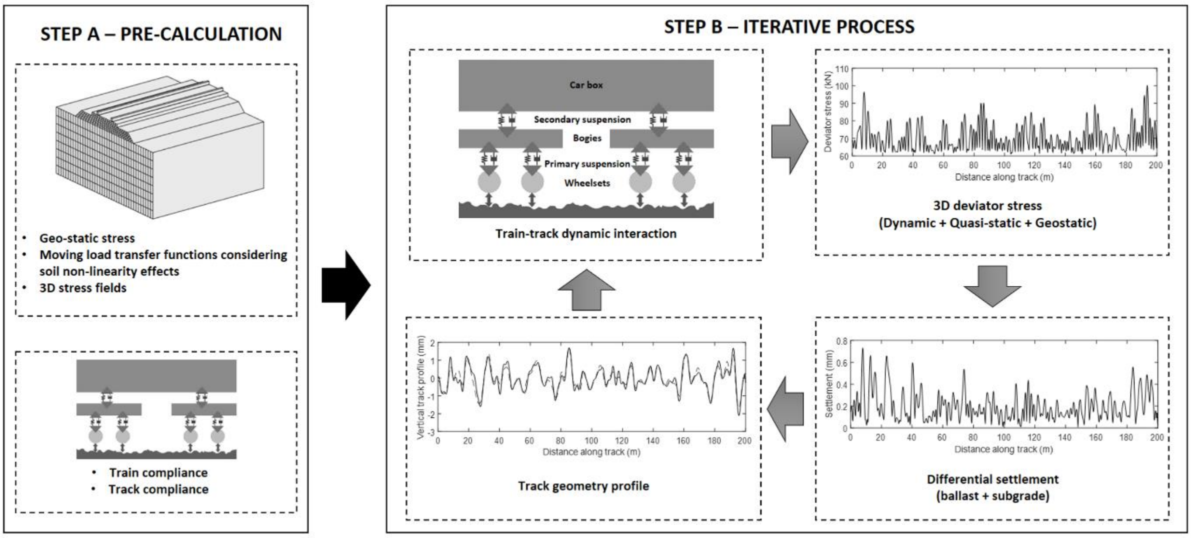

Figure 1. Model overview

4. Numerical model description

4.1.1.General formulation

The wavenumber finite element method (aka two-and-a-half dimension approach) is a computationally efficient method for the solution of three-dimensional domains. Two dimensions are solved via finite element theory while the third is solved analytically. It is therefore well-suited for 3D structures that can be approximated as having invariant geometry and material properties in one direction (e.g. railways, highways and tunnels). An example discretisation of the track-ground structure using the developed mesh generator is illustrated in Figure 2. This cross-section remains invariable in the longitudinal direction of the track, however the loading is 3D and the track-ground response is calculated in 3D. The interactions between different interfaces/layers are modelled accounting for the continuity of displacements and equilibrium of stresses along each subdomain interface (François et al., 2010).

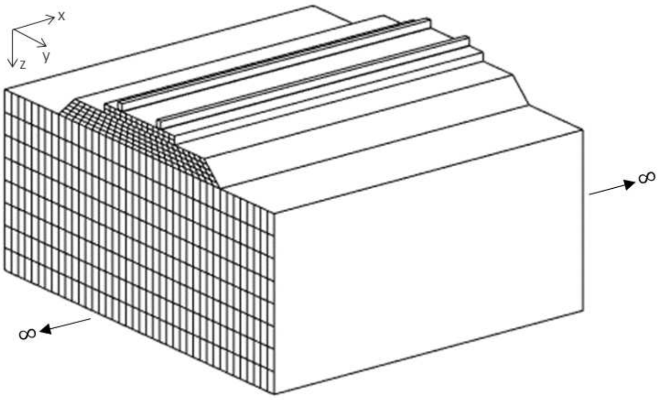

Figure 2. Infinite and invariant structure in the x direction

Assuming the structure is linear and elastic, the equations of motion can be solved in the wavenumber-frequency domain. A double Fourier transform is used to transform all variables into the wavenumber-frequency domain in terms of the moving direction of the train (x direction) and time (t).

Following a general finite element formulation, the following equilibrium equation represents any point in the 3D domain:

$$\int_V \delta\varepsilon\sigma \, dV + \int_V \delta u\rho \frac{\partial^2 u_i(x,t)}{\partial t^2} dV = \int_S \delta up \, dS \tag{1}$$

where $\delta\varepsilon$ is the virtual strain field; σ is the stress field; δu is the virtual displacement field; u is the displacement field; ρ is the mass density; and p is the applied load.

Eq. (1) can be rewritten in terms of nodal variables because the untransformed domain cross-section is discretised into finite elements. Then, considering Parseval's theorem (Hardy and Littlewood, n.d.), the concept of virtual work is applied to the transform domain. The functions of the Fourier images of x and t are defined as wavenumber and frequency denoted by k_x and ω, respectively. Therefore, in the transformed domain, the virtual work of the internal stresses and inertial forces is:

$$\int_V \delta\varepsilon\sigma \, dV = \int_{k_x} \delta u_n^T(-k_x,\omega) \int_z \int_y B^T(-k_x) D B(k_x) \, dy \, dz u_n(k_x,\omega) \, dk_x \tag{2}$$

$$\int_V \delta u\rho \frac{\partial^2 u(x,t)}{\partial t^2} dV = -\omega^2 \int_{k_x} \delta u_n^T(-k_x,\omega) \int_z \int_y N^T \rho N \, dy \, dz u_n(k_x,\omega) \, dk_x \tag{3}$$

where B is the matrix containing the derivatives of the finite element shape functions; D is the elasticity matrix; N is the shape function matrix; and u_n is the nodal displacement vector in the transformed domain.

Taking advantage of the finite element discretisation on the YZ plane and considering a coordinate 'S' parallel to the edge the element where traction is applied, the virtual work induced by the load is:

$$\int_S \delta up \, dS = \int_{k_x} \delta u_n^T(-k_x,\omega) \int_S N^T p(k_x,\omega) \, ds \, dk_x = \int_{k_x} \delta u_n^T(-k_x) p_n(k_x,\omega) \, dk_x \tag{4}$$

Then, substituting Eqs. (2)-(4) into Eq. (1), the equilibrium of each finite element in the YZ plane is:

$$\left(\int_z\int_y B^T(-k_x)DB(k_x)\,dy\,dz - \omega^2\int_z\int_y N^T\rho N\,dy\,dz\right)u_n(k_x,\omega) = p_n(k_x,\omega) \tag{5}$$

Considering classic finite element notation, the stiffness $[K]$ and mass $[M]$ matrices are:

$$[K] = \int_z\int_y B^T(-k_x)DB(k_x)\,dy\,dz \tag{6}$$

$$[M] = \int_z\int_y N^T\rho N\,dy\,dz \tag{7}$$

The matrix $[B]$ is derived from the differential operator matrix $[L]$ and the shape function matrix $[N]$. The longitudinal direction x is transformed into the wavenumber domain, meaning the derivatives in direction x, represented by k_x, are computed analytically.

$$[L] = \begin{bmatrix} ik_x & 0 & 0 & \frac{\partial}{\partial y} & 0 & \frac{\partial}{\partial z} \\ 0 & \frac{\partial}{\partial y} & 0 & ik_x & \frac{\partial}{\partial z} & 0 \\ 0 & 0 & \frac{\partial}{\partial z} & 0 & \frac{\partial}{\partial y} & ik_x \end{bmatrix}^T \tag{8}$$

In terms of damping, a hysteretic damping model is implemented in the frequency domain method via a complex stiffness. The stiffness matrix $[K]$ can be divided into several sub-matrices, independent of the wavenumber (k_x) and frequency (ω) to improve the computation effort. After separating the numerical and analytical derivatives, Eq. (5) is defined as:

$$([K_1] + ik_x[K_2] + k_x^2[K_3] - \omega^2[M])\{u_n\} = \{p_n\} \tag{9}$$

Assuming the system is symmetrical along its centreline, discretisation can be implemented considering only half of the domain. After solving the global system of equations, the displacements in the transformed domain require a double inverse Fourier transform in order to obtain a solution in the space-time domain.

4.1.2. Sleeper elements

The 2.5D method assumes invariant geometry in the direction of train passage. Although the approximation of discrete sleepers using an equivalent continuous formulation gives acceptable results for the frequency range of study (Knothe and Wu, 1998), to maximise accuracy an anisotropic constitutive material model is used to account for discrepancies in bending stiffness.

To do so, the approach proposed by Alves Costa et al. (Alves Costa et al., 2010) and Karlstrom and Bostrom (Karlström and Boström, 2006) is used. The sleepers are modelled as continuous and orthotropic elements, where the physical properties of the sleepers are used in the cross-section. To do so, in the longitudinal plane, the stiffness is set as close to zero. Therefore, the elasticity matrix $[D]_{sleeper}^{-1}$ used to simulate the sleeper elements is:

$$[D]_{sleeper}^{-1}=\begin{bmatrix} \frac{1}{E_x} & -\frac{\nu_{xk}}{E_k} & -\frac{\nu_{xk}}{E_k} & 0 & 0 & 0 \\ -\frac{\nu_{xk}}{E_x} & \frac{1}{E_x} & -\frac{\nu_{kk}}{E_k} & 0 & 0 & 0 \\ -\frac{\nu_{xk}}{E_x} & -\frac{\nu_{kk}}{E_k} & \frac{1}{E_x} & 0 & 0 & 0 \\ 0 & 0 & 0 & \frac{1}{G_{xk}} & 0 & 0 \\ 0 & 0 & 0 & 0 & \frac{1}{G_{kk}} & 0 \\ 0 & 0 & 0 & 0 & 0 & \frac{1}{G_{xk}} \end{bmatrix} \tag{10}$$

$$G_{kk}=\frac{E_k}{2(1+\nu_{kk})} \tag{11}$$

where E_k is the Young's modulus of the sleepers in the isotropic YZ plane; ν_{kk} is Poisson's ratio of the sleeper in the isotropic YZ plane; G_{kk} is the shear modulus in the isotropic YZ plane; E_x is Young's modulus of the sleepers in the track direction; ν_{xk} is Poisson's ratio of the sleeper in the track direction; and G_{xk} is the shear modulus in the track direction.

4.1.3. Rail and rail pad elements

The rails are Euler-Bernoulli beams supported by rail pads which are modelled as springs and dampers connected to the sleeper, as illustrated in Figure 3. Since the beam is defined in the longitudinal direction of the track, the system of equations can be analytically computed in the frequency-wavenumber domain without numerical discretisation and integration, using:

$$\left(\left[K_1^{railpad}\right]+k_x^4\left[K_2^{rail}\right]-\omega^2\left[M^{rail}\right]\right)\{u_n\}=\{p_n\} \tag{12}$$

$$\left[K_1^{railpad}\right]=\begin{bmatrix} k_p^* & -k_p^* \\ -k_p^* & k_p^* \end{bmatrix} \tag{13}$$

$$\left[K_2^{rail}\right]=\begin{bmatrix} EI_r & 0 \\ 0 & 0 \end{bmatrix} \tag{14}$$

$$\left[M^{rail}\right]=\begin{bmatrix} m_r & 0 \\ 0 & 0 \end{bmatrix} \tag{15}$$

where EI_r is the bending stiffness of the rail; m_r is the mass per unit length of the rail; and k_p^* is the complex stiffness of the rail pad taking rail pad's damping into account. In this case, $k_p^*=k_p+i\omega c_p$, where k_p is the stiffness of the rail pad and c_p is the viscous damping factor of the rail pad; $\{u_n\}$ is the vectors that collect the vertical displacements of the rail and rail pad or sleeper components.

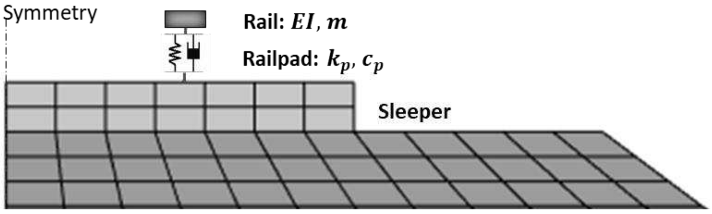

Figure 3. Rail-sleeper connection

Taking into account the global system of equations, the rail pad stiffness in $\left[K_1^{railpad}\right]$ and the rail mass per unit length in $\left[M^{rail}\right]$ can be assembled with the matrices $[K_1]$ and $[M]$ in Eq. (9) respectively. The imaginary part of the matrix $\left[K_1^{railpad}\right]$ is collected in order to form a damping matrix defined as $[C]$. After assembling the element stiffness matrices, the generalised 2.5D finite element equilibrium equation is given by:

$$([K_1] + ik_x[K_2] + k_x^2[K_3] + k_x^4[K_4] + i\omega[C] - \omega^2[M])\{u_n(k_x, \omega)\} = \{p_n(k_x, \omega)\} \tag{16}$$

4.1.4. Perfectly matched layers

The excitation induced by the passage of the train can be decomposed into two main components: (i) quasi-static load, resulting from the weight of the train; (ii) dynamic load, due to the dynamic interaction between the wheel and the rail. In comparison to the quasi-static load (at speeds below critical velocity), dynamic loading generates propagating waves in the ground and thus high performance absorbing boundaries are needed to prevent domain boundary reflections. Perfectly matched layers consist of layers of elements with identical material properties to the region of the domain they bound. Each sub-layer within the PML domain acts to dampen outgoing waves, and therefore the combined effect of multiple sub-layers is an efficient way to maximise performance. An example setup is shown in Figure 4, where the cross section of the 2.5D model is discretised into finite elements and bounded by adding external layers that are formed by PML's. The waves impinging the boundary between each domain are described by the 2.5D FEM and the 2.5D PML. The PML mesh is 1m thick and divided into 6 sub-layers.

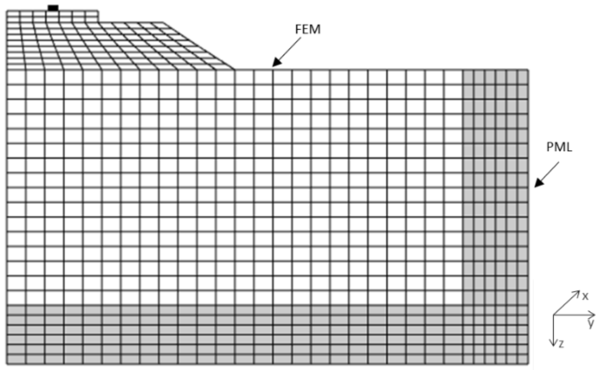

Figure 4. Representative half-track model with PML

The x coordinate is transformed to the wavenumber domain, and thus only the coordinates y and z are stretched by the PML in the complex domain. To allow for the absorption of waves inside the PML domain, the same differential equations used in the FEM domain are modified by considering stretched coordinates $\tilde{y}$ and $\tilde{z}$:

$$\tilde{y} = \int_0^y \lambda_y(y)\, dy \tag{17}$$

$$\tilde{z} = \int_0^z \lambda_z(z)\, dz \tag{18}$$

The non-zero complex valued stretching functions in the y direction (λ_y) and in the z direction (λ_z) are defined using functions:

$$\lambda_y(y) = \frac{2\pi}{|k|}\frac{y}{H_y} - i\frac{k_0}{k}\left(\frac{y}{H_y}\right)^2 \tag{19}$$

$$\lambda_z(z) = \frac{2\pi}{|k|}\frac{z}{H_z} - i\frac{k_0}{k}\left(\frac{y}{H_z}\right)^2 \tag{20}$$

where k_0 is a constant (e.g. Lopes et al. (Lopes et al., 2014) recommend $k_0 = 20$); H_y is the thickness of the PML in the y direction; H_z is the thickness of the PML in z direction; and k is the effective wavenumber for waves propagating along the cross-section, which is given by:

$$k = \sqrt{\left(\frac{\omega}{C_s}\right)^2 - k_x^2} \tag{21}$$

where C_s is the velocity of shear wave.

The coordinates y and z in the equilibrium equation are replaced by $\tilde{y}$ and $\tilde{z}$ respectively. The partial derivatives with respect to $\tilde{y}$ and $\tilde{z}$ are expressed using the following relationships:

$$\frac{\partial}{\partial \tilde{y}} = \frac{1}{\lambda_y(y)}\frac{\partial}{\partial y} \tag{22}$$

$$\frac{\partial}{\partial \tilde{z}} = \frac{1}{\lambda_z(z)}\frac{\partial}{\partial z} \tag{23}$$

Since the solution within the PML domain satisfies the same differential equation as in the 2.5D domain, the stiffness and mass matrices for the PML region can be derived from Eq. (6) and Eq. (7) respectively. The differential operator $[L^*]$ is given by:

$$[L^*] = \begin{bmatrix} ik_x & 0 & 0 & \frac{1}{\lambda_y(y)}\frac{\partial}{\partial y} & 0 & \frac{1}{\lambda_z(z)}\frac{\partial}{\partial z} \\ 0 & \frac{1}{\lambda_y(y)}\frac{\partial}{\partial y} & 0 & ik_1 & \frac{1}{\lambda_z(z)}\frac{\partial}{\partial z} & 0 \\ 0 & 0 & \frac{1}{\lambda_z(z)}\frac{\partial}{\partial z} & 0 & \frac{1}{\lambda_y(y)}\frac{\partial}{\partial y} & ik_x \end{bmatrix}^T \tag{24}$$

Due to the frequency dependence of the stretching functions inside the PML domain, the equilibrium condition after assembling the equations of each individual element is:

$$\left(\left[K_{FEM}^{global}(k_x)\right] + \left[K_{PML}^{global}(k_x,\omega)\right] - \omega^2\left(\left[M_{FEM}^{global}\right] + \left[M_{PML}^{global}(k_x,\omega)\right]\right)\right)\{u_n(k_x,\omega)\} = \{p_n(k_x,\omega)\} \tag{25}$$

where $\left[K_{FEM}^{global}\right]$ and $\left[K_{PML}^{global}\right]$ are the global stiffness matrices of the FEM and PML domains respectively, and $\left[M_{FEM}^{global}\right]$ and $\left[M_{PML}^{global}\right]$ are the mass matrices of the FEM and PML domains respectively.

4.1.5.Soil stiffness non-linearity

When train speed is high and/or axle loads are heavy, large strains can be induced in the soil, and thus the probability of non-linear stiffness behaviour increases (Dong et al., 2019; Shih et al., 2017). This behaviour effects stress wave generation and propagation, and thus settlement, meaning it is important to capture.

The typical stress-strain behaviour of track and ground during cyclic loading can be described by a nonlinear hysteretic loop (Hardin and Drnevich, 1972). This causes the soil stiffness to decrease and the damping ratio to increase as strain increases. To assess non-linear behaviour in the frequency domain while minimising computational demand, an equivalent linear approach is used. The shear modulus reduction curve and the damping ratio are based on an empirical equation proposed by (Ishibashi and Zhang, 1993) which requires cyclic shear strain amplitude (γ_{eff} in this case), mean effective confining pressure and the soil's plasticity index as inputs. Regarding the embankment material, the relationship proposed by (Rollins et al., 2020a) is used.

An iterative procedure based on the effective octahedral shear strain is used to update the properties of each element until agreement between the material properties and strain-adjusted properties is achieved. This implementation can be summarised in the following steps:

1. Start calculation assuming low strain properties for all elements
2. Use Eq. (26) to compute the effective octahedral shear strain from strain time histories and select the maximum value for each element
3. Use the maximum values of the effective octahedral shear strain with stiffness-strain relationship and damping-strain relationship curves (e.g. Figure 9) to compute new equivalent linear values, and update the stiffness and the damping of each element in anticipation of the next iteration. Note that for unbounded soil regions, PML elements are updated using the properties from the closest elements within the intersecting FE domain
4. Repeat steps 2-3 until the differences between both the shear modulus and damping in successive iterations fall below 3% for all elements (Alves Costa et al., 2010)

As the model is used to calculate 3D stress fields, the effective octahedral shear strain is computed as:

$$\gamma_{eff} = \alpha \frac{1}{3} \sqrt{\left(\varepsilon_x - \varepsilon_y\right)^2 + (\varepsilon_x - \varepsilon_z)^2 + \left(\varepsilon_y - \varepsilon_z\right)^2 + 6\left(\gamma_{xy}^2 + \gamma_{xz}^2 + \gamma_{yz}^2\right)} \tag{26}$$

where α is 0.65 (as typically used in seismic analysis); ε_x, ε_y and ε_z are the strains in three directions; and γ_{xy}, γ_{xz} and γ_{yz} are the corresponding shear strains. The non-linear calculation procedure is performed during Step A and the strain-adjusted material properties are passed to Step B for settlement calculation.

4.2. Train-track interaction

Accurately simulating vehicle dynamics and train-track interaction is vital for differential settlement prediction. This is because it is the interaction between wheel and rail that induces differing dynamic forces along the track, that create track-ground stresses, which in turn govern settlement. To simulate this, vehicle-track interaction is solved using a compliance procedure formulated in a moving frame of reference, subject to a moving train (Colaço et al., 2016; Costa et al., 2012). As vertical differential settlement is the parameter under investigation, only vertical dynamics are considered.

4.2.1. Vehicle model

The equilibrium equations for the vehicle and the track are formulated separately. Then the interaction forces between these two structural systems are calculated respecting equilibrium conditions and displacement compatibility at the connecting points. Assuming perfect contact between train and track, any temporal instant for all connection points between the wheel and the rail is fulfilled by:

$$u_{c,i} = u_r\left(t = \frac{x-a_i}{v_0}\right) + u_{irr}\left(t + \frac{a_i}{v_0}\right) + \frac{P_{dyn,i}(t)}{k_H} \tag{27}$$

where u_r is the vertical displacement of the rail; $u_{c,i}$is the vertical displacement at the contact point i; a_i is the location of the contact point i; v_0 is the moving speed of the vehicle; t is the time; u_{irr} is the vertical track irregularity; $P_{dyn,i}$ is the dynamic interaction load at the contact point i; and k_H is the Hertzian stiffness.

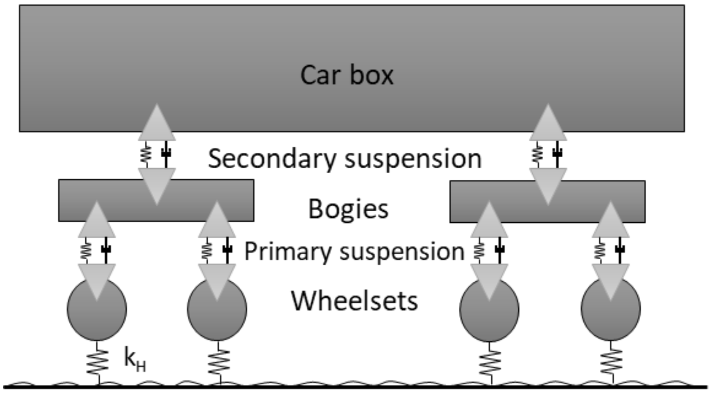

Figure 5. Multi-body vehicle model

A rigid multi-body vehicle model with two levels of suspension, as proposed by Zhai and Cai (Zhai and Cai, 1997) is considered (Figure 5). Since the analysis is performed in the frequency domain, Eq. (27) can be formed in the frequency domain using the transformation of the unevenness track for that domain. Therefore, the dynamic interaction forces in the frequency domain are:

$$\{F_{dyn}(\Omega)\} = -([V] + [V^H] + [T])^{-1}\{\Delta u(\Omega)\} \tag{28}$$

$$\{\Delta u(\Omega)\} = \delta u\{b(\Omega)\} \tag{29}$$

$$b(\Omega)_i = e^{i\frac{2\pi}{\lambda}a_i} \tag{30}$$

$$T(\Omega) = \frac{1}{2\pi}\int_{-\infty}^{+\infty} u_c^G(k_x, \omega)dk_x \tag{31}$$

$$V^H = \frac{1}{k_H} \tag{32}$$

$$V(\Omega) = [Z]([K^v] - \Omega^2[M^v])^{-1}[Z]^T \tag{33}$$

where Ω is the driving frequency, defined by $\Omega = \frac{2\pi}{\lambda}v_0$; T is the flexibility term of the track compliance; V is the flexibility term of the vehicle compliance; V^H is the contact flexibility matrix; Z is a constant matrix, M^v is the vehicle mass matrix and K^v is the vehicle stiffness.

The mass and stiffness matrices of the vehicle system with primary and secondary suspensions are given in the Appendix.

Regarding the Hertzian stiffness, since the dynamic portion of the contact force is typically substantially less than the static action (weight of the train per wheel), the contact stiffness can be linearised considering only the portion of the force P corresponding to the distribution of the weight of the train per wheel (Sheng et al., 2003; Wu and Thompson, 2001). Therefore, a linearization procedure can be adopted, in which only the dead load transmitted by the wheelset is taken into account (Kouroussis et al., 2014). The linearised (Hertzian) contact stiffness is defined as:

$$k_H = \frac{3}{2G} {P_0}^{1/3} \tag{34}$$

where P_0 is the static load transmitted by the wheel to the rail; and G is the contact constant depending on the radius and geometry of the wheel, and rail bearing surface.

4.2.2. Track irregularities

The geometric irregularity of the track can be defined using either a synthetic profile or from data gathered by an in-service measurement vehicle. Track irregularities can be described using power spectral density (PSD) as a function of spatial frequency, of which there are various formulations. The formulation used in this work is based on the Federal Railway Administration (FRA) which divides the track into different classes for the quantification of track unevenness (Federal Railroad Administration, 1980).

In contrast to artificial track irregularities, measured irregularity profiles can also be used for simulating dynamic excitation. The raw signals from measurement are band-pass filtered to obtain signal wavelengths within the interested range. In addition, the signals are proceeded using a transformation from the space domain into the spatial frequency domain, since the analysis is conducted in the frequency domain. Instead of using the Fourier Transform, it is necessary to take into account the discrete nature of the digital signals. Therefore, a Discrete Fourier Transform is applied (Cooley and Tukey, 2019) to deal with the domain transformation process of the measured track irregularity profile.

4.3. Permanent strain and settlement models

4.3.1. Ballast settlement

The ballast settlement model is inspired by the ORE-type formulation (ORE, 1970) which depends upon the number of loading cycles, deviator stress and ballast porosity. The empirical constants are adjusted to improve the fit with the experimental data generated by (Abadi et al., 2016). Figure 6 shows curve fits from the proposed equation and the experimental data in the settlement rate, against the logarithm of the number of load cycles. It should be noted that the permanent strain during the first cycles is removed to avoid any effects due to the initial rapid rearrangement of ballast particles during lab testing. The proposed equation shows a strong fit with the experimental data.

A key advantage of using an iterative modelling approach is that the differential settlement and track profile can be updated after every load passage. However, this requires that the deviatoric stress must also be recalculated after every passage. Further, the equation must be able to compute settlement for varying scenarios, including:

1. The case of newly constructed or renewed/tamped track, where the ballast has only experienced minimal loading
2. The case of existing ballast, where the ballast has previously been compacted under a large volume of traffic

Considering these factors and the need to regularly update the track profile, an alternative form of the ORE settlement equation is required, that is able to account for the settlement of previous axle passages in its calculation. Therefore a modified permanent strain equation, computed at every iterative step is proposed:

$$\begin{aligned}\Delta\varepsilon_{p\_b,i} = 0.375\left(\sigma_{d\_b,i}\right)^2 & \\ \times \big[\left(1 + 0.4\,log_{10}\left((dN \cdot i) + N_{lb}\right)\right) & \\ - \left(1 + 0.4\,log_{10}\left((dN \cdot (i-1)) + N_{lb}\right)\right)\big] &\end{aligned} \tag{35}$$

The corresponding settlement is then:

$$\Delta S_{b,i} = \sum_{j=1}^{k} \Delta\varepsilon_{p\_b,i_j} \cdot h_j \tag{36}$$

where $\Delta\varepsilon_{p\_b,i}$ is ballast permanent strain increment; i is iterative step; $\sigma_{d\_b,i}$ is ballast dynamic deviatoric stress relevant to traffic load (in MPa); N_{lb} is the number of load cycles after the last ballast renewal/tamping; $\Delta S_{b,i}$ is ballast settlement increment; h_j is the thickness of each layer; k is number of sublayers. dN is the frequency of load application, for example where $dN = 1$ indicates every load passage is simulated, and $dN = 1000$ indicates every 1000th load passage is simulated.

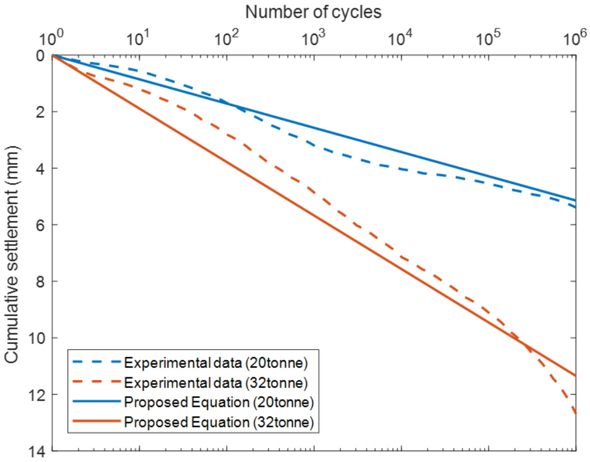

Figure 6. Comparison of proposed ballast settlement model with experimental data

4.3.2. Subgrade settlement

The subgrade settlement equation is a modified version of that proposed by Li and Selig (Li and Selig, 1996). Similar to the approach for calculating ballast settlement, it is modified to take into account the evolution of dynamic stress and to allow for the simulation of both newly constructed track and existing subgrade. The proposed, modified permanent strain increment and settlement increment at each iterative step are:

$$\Delta\varepsilon_{p\_s,i} = \frac{a}{100}\left(\frac{\sigma_{d\_s,i}}{\sigma_s}\right)^m \left[\left((dN\cdot i)+N_{ls}\right)^b - \left((dN\cdot(i-1))+N_{ls}\right)^b\right] \tag{37}$$

$$\Delta S_{s,i} = \sum_{j=1}^{k} \Delta\varepsilon_{p\_s,i_j}\cdot h_j \tag{38}$$

where $\Delta\varepsilon_{p\_s,i}$ is subgrade permanent strain increment; $\sigma_{d\_s,i}$ is subgrade dynamic deviatoric stress relevant to traffic load (in Pa); σ_s is soil compressive strength (in Pa); N_{ls} is the number of load cycles after the last subgrade replacement; $\Delta S_{s,i}$ is subgrade settlement increment; and a, m, and b are material parameters given in Table 1.

Table 1 Settlement parameters a, b, and m for various subgrade soil types (Li and Selig, 1996)

Material parameter	**High-plasticity clay (CH)**	**Low-plasticity clay (CL)**	**High-plasticity silt (MH)**	**Low-plasticity silt (ML)**
a	1.20	1.10	0.84	0.64
b	0.18	0.16	0.13	0.10
m	2.40	2.00	2.00	1.70

Figure 7 illustrates example settlement rates for three different cases. Figure 7(a) is the case of new track construction (newly placed ballast and soft subgrade) where a soft subgrade provides higher settlement than the ballast in the years after construction. Alternatively, Figure 7(b) is where the track has been compacted under several years of traffic loading, but the ballast has recently been renewed. In this case the ballast settlement exceeds the subgrade, particularly in the initial period after tamping. The third case, as seen in Figure 7(c), shows when the ballast and subgrade have both been in place for many years. The deformation rates of both ballast and subgrade increase slowly with increased load passages.

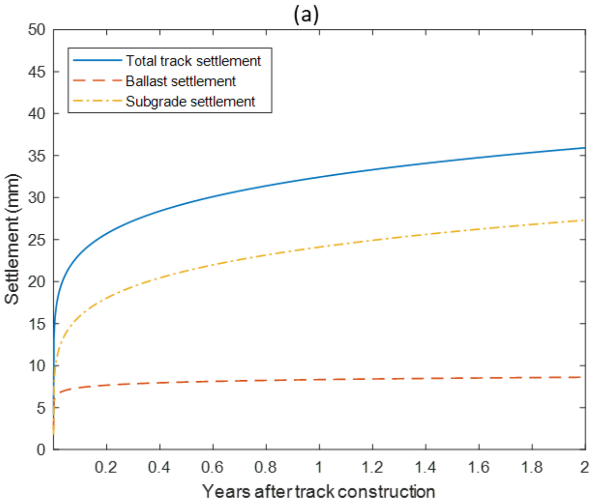

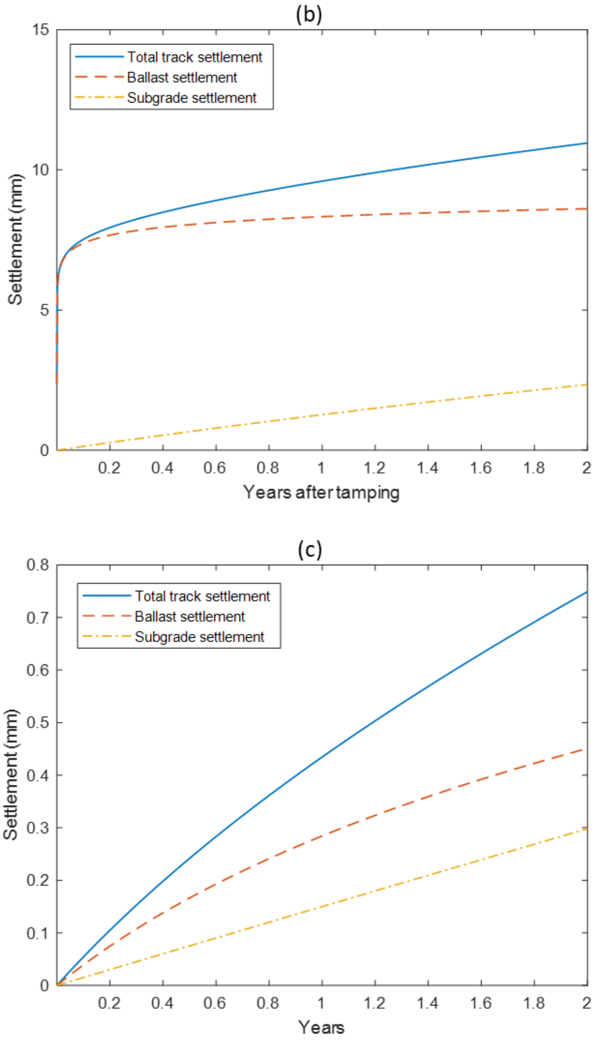

Figure 7. Ballast, subgrade, and total track settlement: (a) a newly constructed track (b) an existing track following tamping and (c) an existing track that has not recently been tamped

4.3.3. Geostatic stress

In addition to the stresses induced by quasi-static and dynamic loads, the stress field due to geostatic loading is also included in the settlement calculation. The vertical stress at a given location is calculated from the mass of the overlying material:

$$\sigma_V = \rho g h_z \tag{39}$$

where σ_V is the vertical stress; ρ is the density of the overlying material; g is gravity; and h_z is the vertical distance from the monitored point to the free surface.

Considering an unsaturated soil, the total stress is equal to the effective stress due to the absence of pore water pressure. The effective horizontal stress is approximated as a proportion of the effective vertical stress:

$$\sigma'_H = K'_0 \sigma'_V \tag{40}$$

$$\frac{\sigma'_H}{\sigma'_V} = K'_o = \frac{\upsilon}{1-\upsilon} \tag{41}$$

where K'_0 is the coefficient of lateral stress (varying between 0 and 1.0).

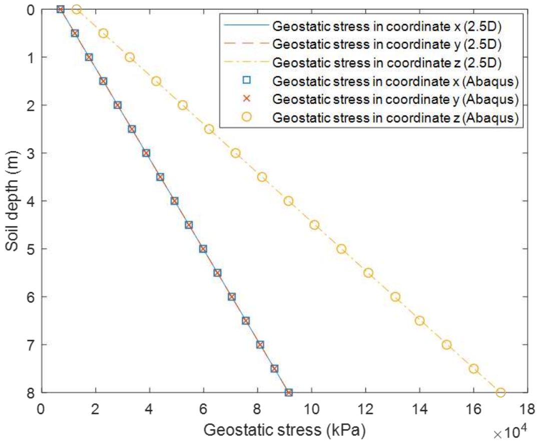

Figure 8. Geostatic stresses at the track centre

To check the accuracy of the geostatic stress calculation in the 2.5D model, geostatic stresses were calculated in the track, at the location of settlement computation. The results are compared with results from a 3D model, simulated using commercial FE software ABAQUS (Figure 8). The result is a strong fit.

Considering the stress field in 3D, the deviatoric stress is dependent on the sum of squares of the differences of the principal stresses:

$$\sigma_d = \sqrt{\frac{1}{2}} \times \sqrt{(\sigma_1 - \sigma_2)^2 + (\sigma_2 - \sigma_3)^2 + (\sigma_3 - \sigma_1)^2} \tag{42}$$

where σ_1, σ_2 and σ_3 are the components of the principal stresses. Note that the total deviatoric stress includes the geo-static, quasi-static and dynamic stress components. It is calculated every 0.2m along track length (in the train passage direction) and at vertical depth intervals of 0.25m.

4.4. Detailed solution procedure

The previous sections outlined the general modelling strategy and key considerations. This section describes how they fit together to form the overall modelling methodology. Firstly, considering the two-step modelling approach (Figure 1), the sub-steps for the implementation of Step A are:

1. Calculate the geostatic stresses over the cross-section of the track structure
2. Determine the strain-adjusted material properties, considering non-linear material stiffness, due to quasi-static loading, using the 2.5D FEM-PML method
3. Compute the moving quasi-static and dynamic load transfer functions
4. Calculate the 3D stresses based on a unit load in the wavenumber-frequency domain
5. Compute the matrices of track compliance and train compliance

Step A only requires computation once, and when complete, the sub-steps for Step B are:

1. Calculate the train-track dynamic interaction forces based on the track irregularity profile and multi-body vehicle

2. Calculate the dynamic stresses along the entire track length. The calculation is performed in the wavenumber-frequency domain and then transformed to obtain the 3D dynamic stress fields in the time-space domain
3. Use the quasi-static, geostatic, and dynamic stresses to compute the deviatoric stress (σ_d) using Eq. (42)
4. Compute the permanent strain increments and the settlement increments in ballast and subgrade layers according to Eqs. (35) and (37) respectively
5. Obtain the differential track settlement over the entire track length
6. Update the track geometry irregularity and perform a domain transformation to convert the updated signal into the spatial frequency domain
7. Return to step 1 and repeat the subsequent steps using the updated track geometry irregularity
8. Stop when threshold reached (e.g. total cycles or standard deviation threshold)

5. Model validation

The following describes three validations confirming model accuracy. Firstly the dynamic track-ground calculation is validated, followed by the train-track interaction forces, and finally differential settlement.

5.1. Validation case 1: Track-ground dynamics and non-linearity

Case 1 is used to validate the model's ability to simulate track-ground dynamics and non-linear behaviour using an iterative linear equivalent procedure. The validation is performed using data from the case of a soft soil site at Ledsgard, Sweden (Madshus and Kaynia, 2000). This site experienced large deflections under the passage of X2000 trains shortly after opening, attributed to critical velocity effects (Connolly et al., 2020; Connolly and Costa, 2020), leading to soil non-linearity.

Regarding the material properties at the site, the UIC60 rail is continuously supported by railpads with a stiffness of 255x10^6 N/m^2 and a damping coefficient of 22.5x10^3 Ns/m^2. The sleepers are simulated using the aforementioned anisotropic constitutive model, with a Young's modulus of 30GPa. The low-strain soil properties are based on field test results and shown in Table 2. The experimental data for organic clay is taken from (Alves Costa et al., 2010). Embankment material properties are based on experimental data from (Dyvik and Kaynia, 2018). Figure 9(a) and (b) show the shear modulus reduction and damping ratio curves obtained using the empirical equations proposed by (Rollins et al., 2020b) for the embankment, and (Ishibashi and Zhang, 1993) for the other soil layers. Train loading information is available in (Dong et al., 2019).

Table 2. Small-strain properties at Ledsgard

Layer	Thickness (m)	Density (kg/m^3)	P-wave speed (m/s)	S-wave speed (m/s)	Damping ratio
Embankment	1.2	1800	210	340	0.04
Dry crust	1.1	1500	63	500	0.04
Organic clay	3.5	1260	41	500	0.02
Clay 1	4.5	1475	60	1500	0.05
Clay 2	6.0	1475	87	1500	0.05

Clay 3	30.0	1475	100	1500	0.05

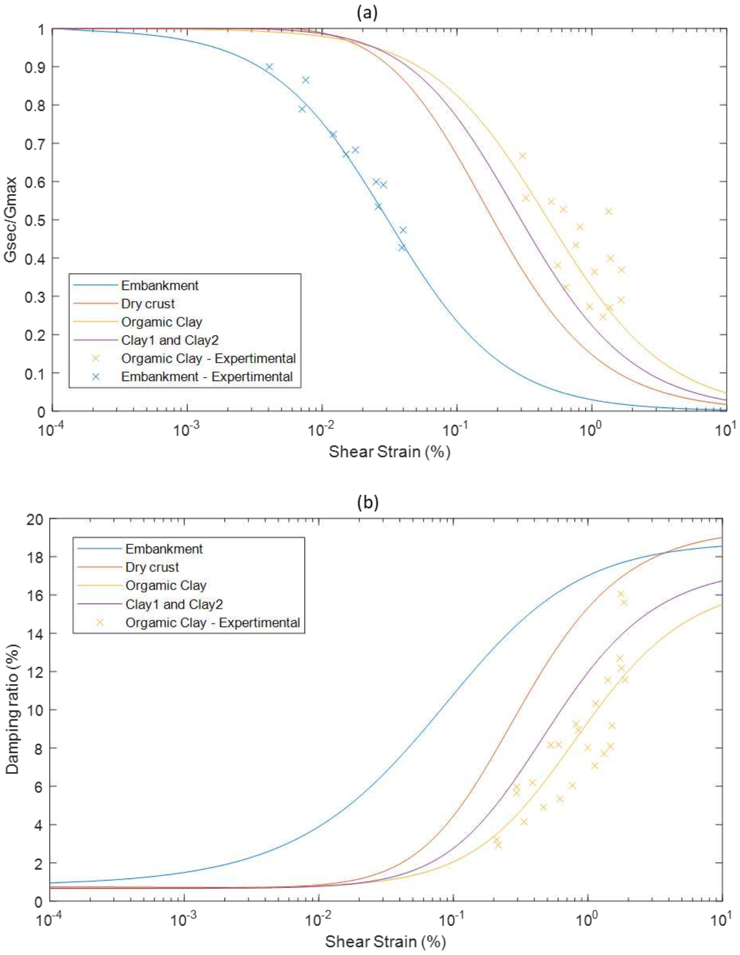

Figure 9. Non-linear soil characteristics (a) shear modulus reduction curves (b) damping ratio

The 3D track-ground displacement contour for a 70km/h train is illustrated in Figure 10. The deflection contours are visible and show the response propagating from the rail into supporting track-ground structure. Figure 11(a) and (b) show the examples of time histories of displacements calculated with and without considering non-linear effects, and compared with the field data for speeds of 70 km/h and 140 km/h, respectively. It can be seen that the results predicted by the non-linear simulation are a significantly better fit than the linear simulation. This is consistent with the works of (Dong et al., 2019) and (Alves Costa et al., 2010), and confirms the model's ability to simulate the non-linear part of the response. Figure 11(c) compares the peak upward and downward displacements between the field data, the linear simulation and the non-linear simulation for speeds ranging from 70 to 205 km/h. The comparison reveals that the results from a non-linear formulation are again a closer match with the field data. Therefore, it can be concluded that the model is capable of accurately calculating railway track deflections, regardless of whether the strain levels induce non-linear behaviour or not.

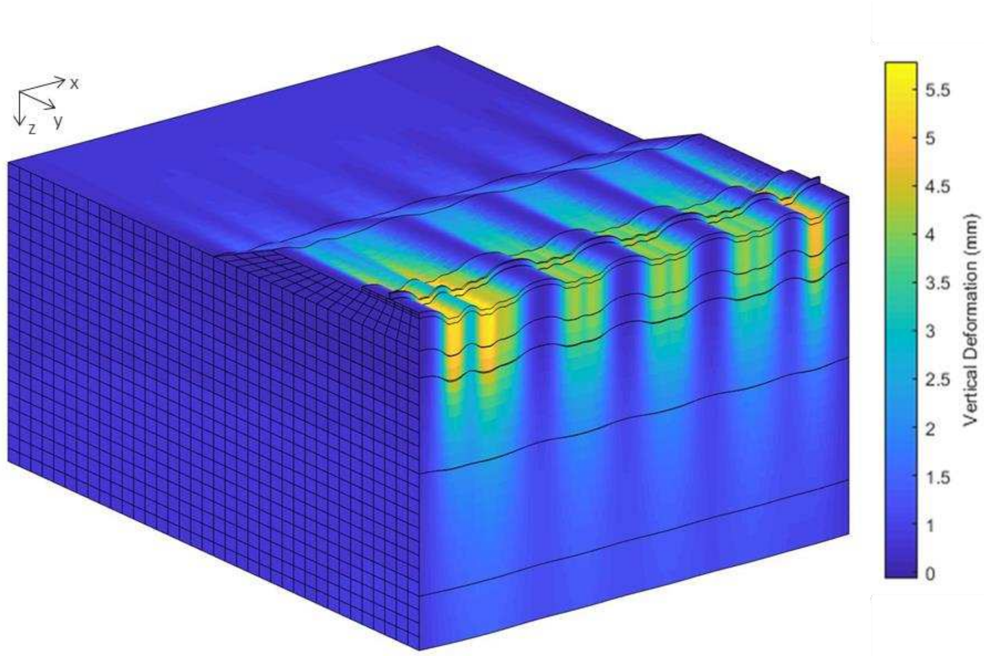

Figure 10. 3D track-ground deflection profile (slice along track centreline)

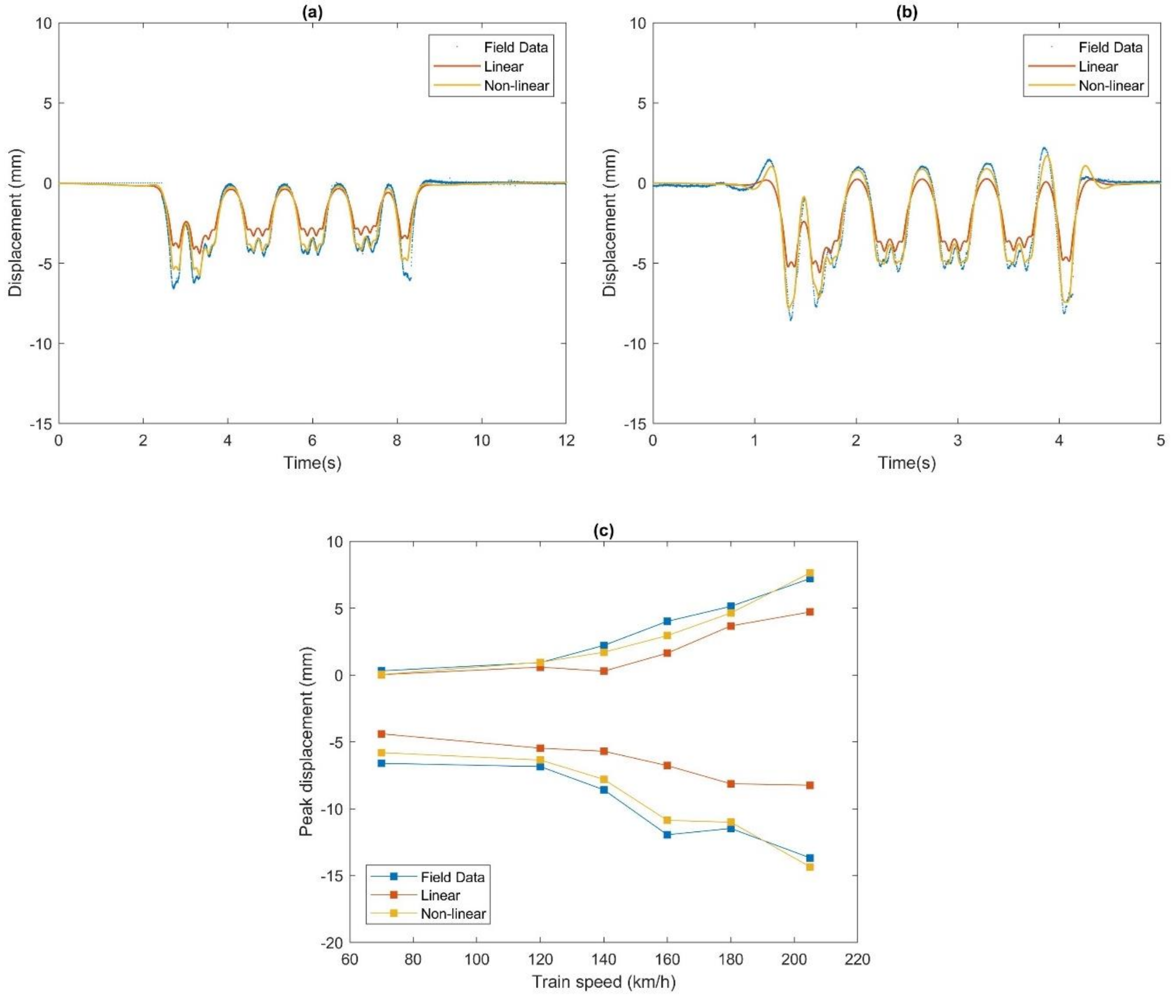

Figure 11. Measured and simulated time histories of track displacements for different train speeds (Southbound): (a) speed = 70km/h (b) speed = 140km/h (c) peak displacements versus train speeds

5.2. Validation case 2: Train-track interaction

Case 2 is used to validate the frequency-wavenumber domain solution method for train-track interaction. This is important for accurately calculating the forces that lead to the stresses in the track-subgrade. The validation is performed using an artificial track irregularity profile defined by FRA (Federal Railroad Administration, 1980) Class 5 for wavelengths in the range $3 < \lambda \leq 25\ m$. The model of train-track dynamic interaction in the frequency domain is validated against an equivalent time domain FE model (Thompson, 2008) solved using an implicit integration scheme. The time domain model is governed by:

$$F_{dyn} = \frac{i\omega r Y_r}{Y_r + Y_w + Y_c} \tag{43}$$

$$Y_r = \frac{i\omega u_{max}}{F_{sta}} \tag{44}$$

$$Y_w = \frac{-i}{\omega M_w} \tag{45}$$

$$Y_c = \frac{i\omega}{k_H} \tag{46}$$

where $i\omega r$ is the roughness velocity amplitude; Y_r is the vertical rail mobility; Y_w is the wheel mobility; Y_c is the contact spring mobility; u_{max} is the maximum displacement due to static load; F_{sta} is the static load; and M_w is the wheelset mass.

The validation is a simplified 2D model of a railway track as shown in Figure 12. The rail is represented using an infinite Euler-Bernoulli beam supported by a single continuous elastic layer. It has the following material properties: Young's modulus $E = 2.1x10^{11}\ N/m^2$; second moment of area $I = 30.55x10^{-6}\ m^4$; cross section area $A = 0.00763\ m^2$; density $\rho = 7850\ kg/m^3$; and support stiffness $s = 1x10^8\ N/m^2$. A single axle vehicle travels across the structure at speed of 150 km/h, with wheel mass $M_w = 2003\ kg$. The load on the wheel (from weight of the vehicle) is $195\ kN$.

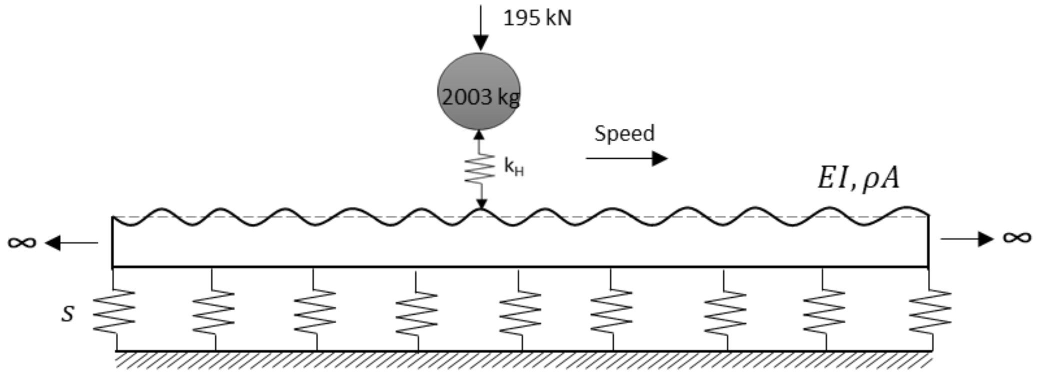

Figure 12. Simplified 2D train-track interaction problem

Figure 13 shows a comparison of displacement time histories between the time domain model and the frequency domain model. It should be noted that the displacements are only due to the dynamic load and not combined with the quasi-static load. A good match of the results confirms the accuracy of the train-track dynamic interaction model.

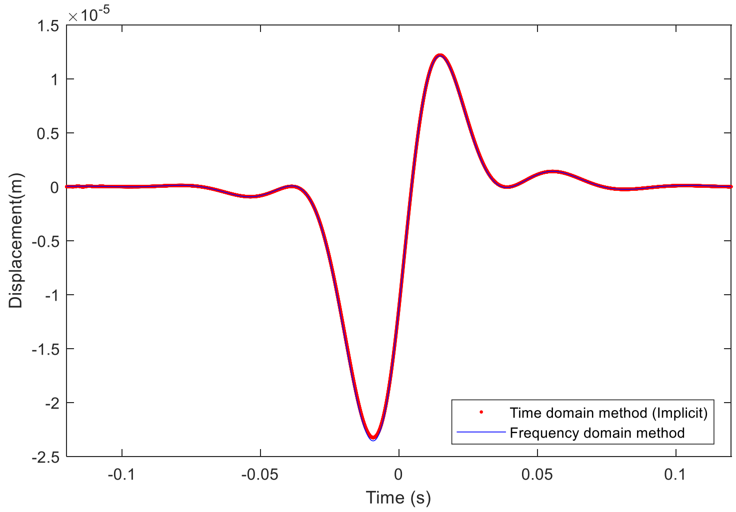

Figure 13. A comparison of displacement time histories due to dynamic loading

5.3. Validation case 3: Differential settlement

Case 3 is used to validate the model's ability to compute the evolution of vertical track geometry with increasing axle passages. Historical track geometry data, from a track section in the UK, is used for comparison. The data was collected using a track recording vehicle, and the standard deviation of the vertical track irregularity profile over a 200m track length is considered. Considering an aim of the model is to predict tamping intervals, only wavelengths in the 3-25m range are considered.

The site investigation data was collated and the properties of the track and subgrade are shown in Table 3. The subgrade is ML soil type (silt) with a shear strength of 25 kPa. The soil strength parameters a, b and m for the subgrade settlement equation are 0.64, 0.10, and 1.7 respectively. The site was specifically selected to have minimal freight traffic, thus reducing the variation in rolling-stock types. The dominant train properties are based upon the British Rail Class 390 Pendolino as shown in Table 4. Regarding the traffic condition, the line speed is 201 km/h with annual tonnage of 37 million gross tonnes (MGT), 98% of which is passenger. Over a year period, track geometry was measured on 04-01-2017, 26-04-2017, 16-08-2017, and 16-12-2017, and no tamping took place between these dates.

Table 3. Ballasted track properties

Component	Parameter	Value
UIC 60 Rail (single rail)	Height (m)	0.172
	Length in transversal direction (m)	0.015
	Section area (m^2)	7.677×10^{3}
	Moment of Inertia y-y (m^4)	3.038×10^{-5}
	Moment of Inertia z-z (m^4)	0.512×10^{-5}
	Young's modulus (Pa)	2.11×10^{11}
	Density (kg/m^3)	7850
	Poisson's ratio	0.3
	Hysteric damping coefficient	0.01
Railpad (spring element)	Continuous stiffness (N/m)	255×10^{6}
	Viscous damping (Ns^2/m)	22.5×10^{3}

Component	Parameter	Value
Sleeper (G44)	Height (m)	0.2
	Length in transversal direction (m)	2.5
	Sleeper spacing (m)	0.65
	Young's modulus (Pa)	3x10^{10}
	Density (kg/m^3)	2500
	Poisson's ratio	0.2
	Hysteric damping coefficient	0.01
Ballast	Height (m)	0.3
	Length in transversal direction (m)	2.8
	Young's modulus (Pa)	97x10^6
	Density (kg/m^3)	1591
	Poisson's ratio	0.12
	Hysteric damping coefficient	0.061
Sub-ballast	Height (m)	0.5
	Length in transversal direction (m)	3.5
	Young's modulus (Pa)	212x10^6
	Density (kg/m^3)	1913
	Poisson's ratio	0.3
	Hysteric damping coefficient	0.054
Subgrade	Young's modulus (Pa)	60x10^6
	Density (kg/m^3)	2000
	Poisson's ratio	0.35
	Hysteric damping coefficient	0.03

Table 4. Pendolino (Class 390) parameters

Parameter	Value
Axle spacing (m)	2.7
Bogie spacing (m)	17
Car body mass (kg)	475x10^2
Car body pitching moment of inertia (kg.m^2)	206x10^4
Bogie mass (kg)	2325
Wheelset mass (kg)	1750
Bogie pitching moment of inertia (kg.m^2)	3000
Primary suspension stiffness (Nm^{-1})	258x10^3
Primary suspension viscous damping (Nsm^{-1})	4250
Secondary suspension stiffness (Nm^{-1})	410x10^3
Secondary suspension viscous damping (Nsm^{-1})	200x10^2

The initial vertical track profile, measured on 04-01-2017 was used as the starting geometry. The model then simulated and updated the track geometry profile, after every individual load passage, based upon expected MGT. Over the course of almost a year, the evolving track geometry profiles are shown in Figure 14. The predicted profile for the final track recording is also shown and compared against the numerical simulation. It is seen that the amplitudes are closely matched in phase and amplitude. There are some discrepancies, however these are most likely due to varying track-ground material properties along the track section, which are difficult to capture from a single-point site investigation, and the fact that the true traffic was not 100% Pendolino rolling stock.

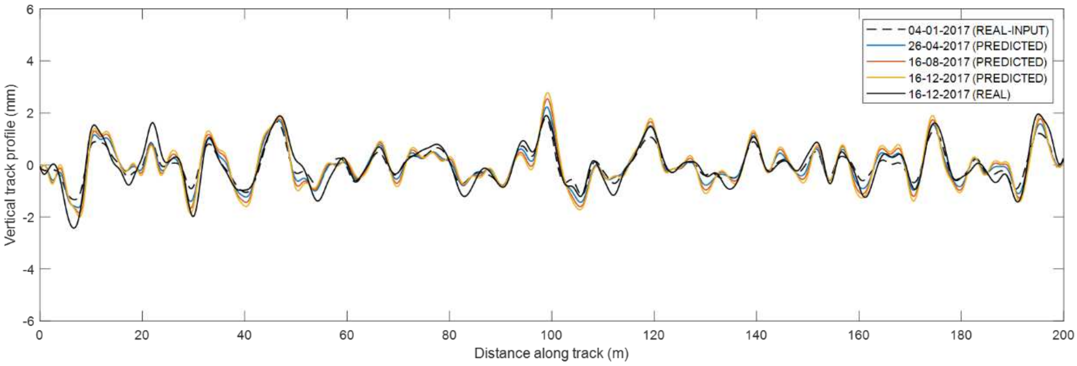

Figure 14. Vertical track profile. Predicted profile vs field data

Figure 15 compares the recorded and predicted evolution of geometry SD at the site. The rectangular markers are the real geometry SD from the recording car, and the red marker is the SD of the initial vertical track profile. The blue solid line is the predicted geometry SD updated after every load cycle during simulation. Compared to the real data, it is seen that the predicted geometry SD curve is a strong match to the recording data. This result, combined with the results in Figure 14, shows the strong ability of the model to accurately predict differential settlement and standard deviation evolution.

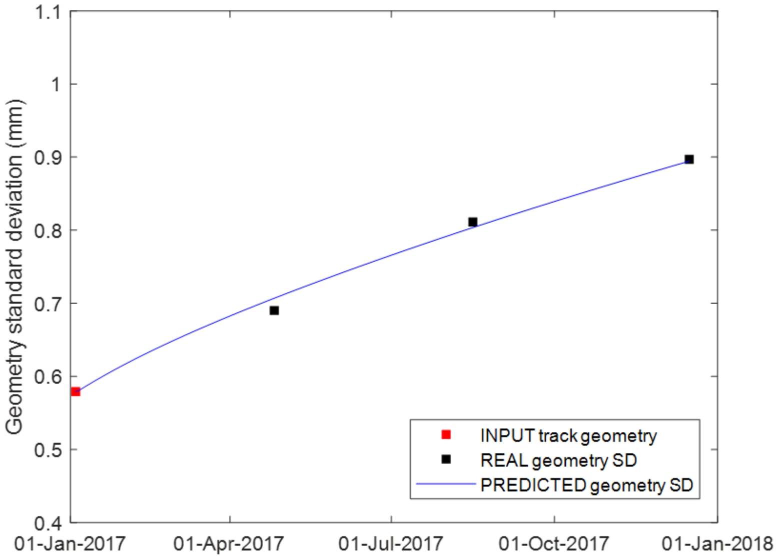

Figure 15. Evolution of standard deviation with time. Predicted values vs field data

6. Analysis

The validated model is used to perform 2 analyses. First it is used to analyse the effect of the frequency of updating track geometry on differential settlement. Three cases are simulated: updating it after every axle passage, updating after every 10 passages, and also after every 100 passages. Secondly, the model is used to investigate the role of settlement parameters in the subgrade settlement model. Four cases are simulated: a low-plasticity silt (ML), a high-plasticity silt (MH), a low-plasticity clay (CL), and a high-plasticity clay (CH). Prior to the analyses the model input properties are defined.

6.1. Model properties

Figure 16 shows the finite element mesh used for the numerical analysis. The characteristics of the rails, rail pads, sleepers, ballast and sub-ballast are the same as described in Table 3. Two different subgrades are considered, with their geotechnical properties shown in Table 5. They are chosen to represent a stiff and soft soil respectively, with Young's modulus being their only differentiating parameter. The vehicle is a Pendolino train travelling at 201 km/h, with properties shown in Table 4.

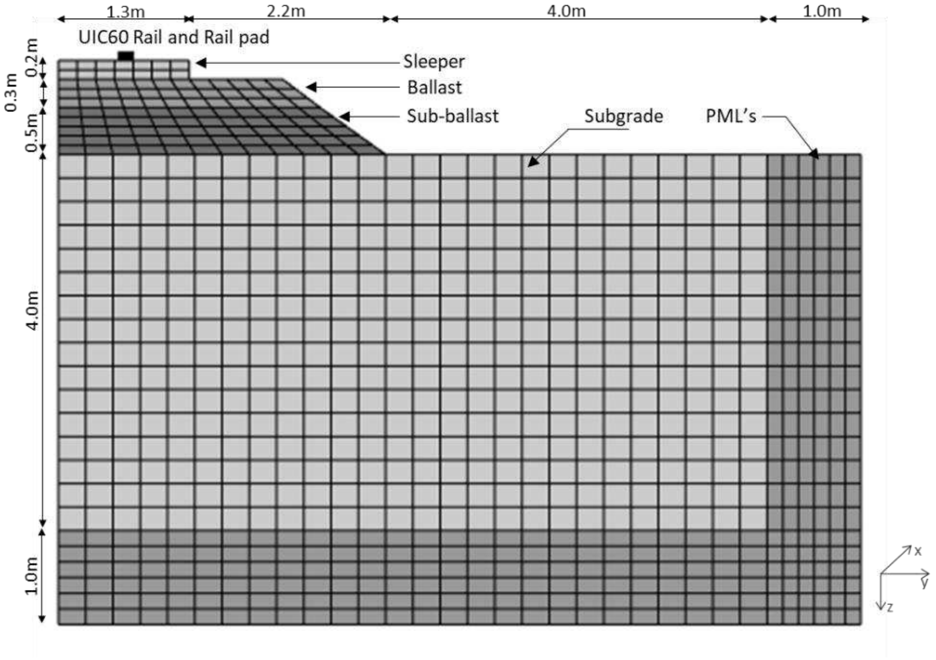

Figure 16. Finite element mesh

Table 5 Subgrade properties

Parameter	Soil case 1	Soil case 2
Young's modulus (Pa)	120×10^6	60×10^6
Density (kg/m^3)	2000	2000
Poisson's ratio	0.3	0.3
Hysteric damping coefficient	0.03	0.03
Primary wave speed (m/s)	284	201
Secondary wave speed (m/s)	152	107

6.2. Track irregularity

A synthetic irregularity profile is used, where the irregularities are generated using a PSD function, where the spatial frequency is $k_x = \frac{2\pi}{\lambda_{irr}}$, and λ_{irr} represents the wavelength of the irregularity. The formulation is based on FRA (Federal Railroad Administration, 1980) and has the following form:

$$S_n(k_x) = \frac{A k_3^2 (k_x^2 + k_2^2)}{k_x^4 (k_x^2 + k_3^2)} \tag{47}$$

where A is a roughness constant, while k_2 and k_3 spatial frequency constants.

After computing the PSD, the amplitude of unevenness in terms of the spatial frequency is:

$$\delta u_j = \left(\sqrt{2 S_n \left(k_{x_j} \right) \Delta k_x} \right) e^{-i\theta_j} \tag{48}$$

where Δk_x is the resolution retained for the spatial frequency, and θ is phase angle, taken as a random variable with uniform distribution in the range 0 to 2π.

Since the track quality is defined using SD over distance along track, the initial track profile in terms of position x is obtained using:

$$u_{irr}(x) = \sum_{j=1}^{N} \delta u_j e^{i k_{x_j} x} \tag{49}$$

6.3. Influence of updating the track geometry after each axle load

To understand how frequently the track geometry profile requires updating between load passage simulations, the two subgrade cases are subject to 100,000 axle loads. The simulations are performed with three different values of: dN=1, 10 and 100. This means the track irregularity profile, train-track dynamic interaction forces, and deviatoric stresses are updated every 1, 10, and 100 load passages until the total number of passages is reached. In practical terms, considering an initial track geometry, dN=100 means that all profile changes due to the next 100 axle loads are not explicitly modelled. Instead, after 100 cycles, the model attempts to update the profile considering the cumulative change due to the previous 100 cycles.

The number of loading applications after the last renewal of ballast and subgrade, N_{lb} and N_{ls}, are equal to zero, representing the case of newly constructed track that has only experienced minimal traffic loading. Both subgrade soils are silty sand, with material parameters (a, m, b) given in Table 1.

The initial track irregularity profile is artificially generated using the PSD function defined by FRA, considering 40 frequencies, and is shown in Figure 17. In order to represent a new track, constructed to tight tolerances and prior to significant train loading, the value of parameter A is set as 0.29x10^{-8} m^2-rad/m.

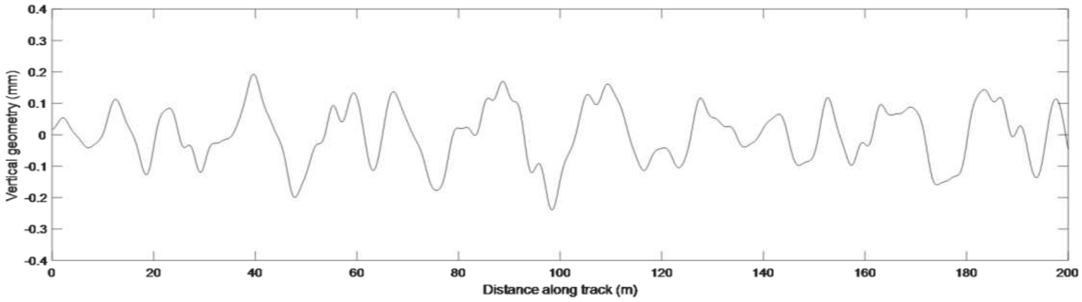

Figure 17. Initial track irregularity profile

Considering Soil case 1 (high stiffness soil), Figure 18(a) shows the change in geometry standard deviation versus load cycles, for dN=1, dN=10, and dN=100. After 100k cycles, it is seen that dN = 1 results in the highest standard deviation, while dN=100 results in the track geometry with lowest standard deviation. The discrepancy between using dN=10 rather than dN=1 is 2.17%, while the discrepancy between using dN=100 rather than dN=1 is 3.62%.

Similar findings are true for Soil case 2 (lower stiffness soil), however the effect is more pronounced, as shown in Figure 18(b). dN=1 results in the highest standard deviation, while dN=100 results in the lowest. The discrepancy between using dN=10 rather than dN=1 is 32.07%, while the discrepancy between using dN=100 rather than dN=1 is 65.43%.

These findings indicate that it is important to update the track geometry profile as frequently as possible, and ideally after every load passage. Although this implies increased computational effort, if not adhered to, then the full effect of train-track interaction on differential settlement is not captured. This is particularly true for softer soils where the effect is amplified.

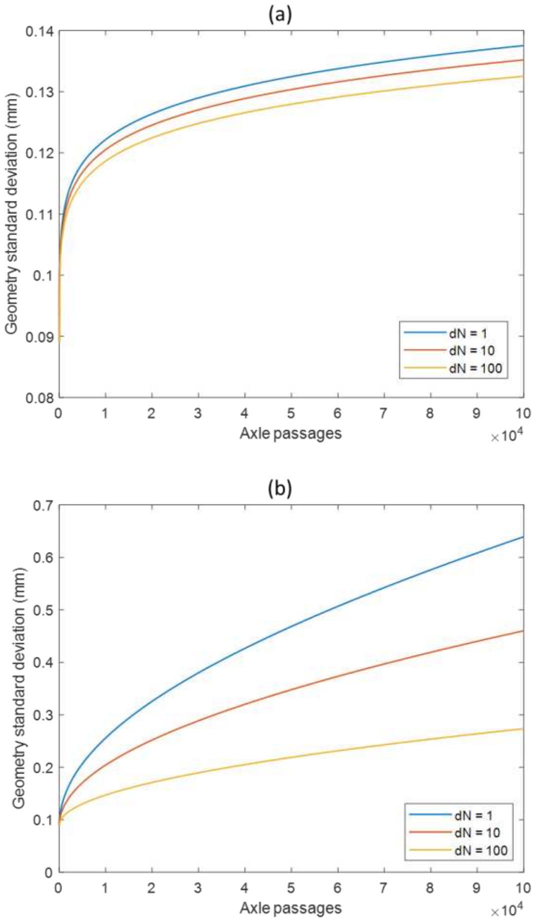

Figure 18. Track geometry evolution versus profile update frequency: (a) high stiffness subgrade; (b) low stiffness subgrade

6.4. Influence of subgrade material properties

The subgrade material model is characterised by: 1) elastodynamic properties, that describe the propagation of stress fields, and 2) settlement properties that describe how these stress fields result in settlement. To understand the relation between these properties, a sensitivity analysis is performed by changing the Young's modulus and also the settlement parameters (a, b and m). The two Young's modulus properties are shown in Table 5, while the four settlement combinations are shown in Table 1. It should be noted that the sensitivity analysis was performed to understand the relationship between parameters, rather than to attempt to simulate any specific soil types.

Figure 19 shows the change in geometry standard deviation versus load cycles, for changing settlement parameters: ML, MH, CL, CH, and for the stiff and soft soils. Considering Soil case 1 (stiff), the standard deviation for a ML soil is 0.149mm. For the other soil types, the standard deviation increases by 4.09%, 7.84% and 16.49% for MH, CL and CH respectively. Similar is true for Soil case 2 (soft), where the same soil types cause increases of 4.74%, 8.38% and 20.66% respectively. Therefore it can be concluded that the higher the clay content in the soil, the larger the settlement. However, although the settlement parameters have a marked difference on track geometry, the difference between the soft and stiff soil is even greater. The soft soil has a significantly higher standard deviation for all settlement parameters, which shows the importance of subgrade stiffness on track performance.

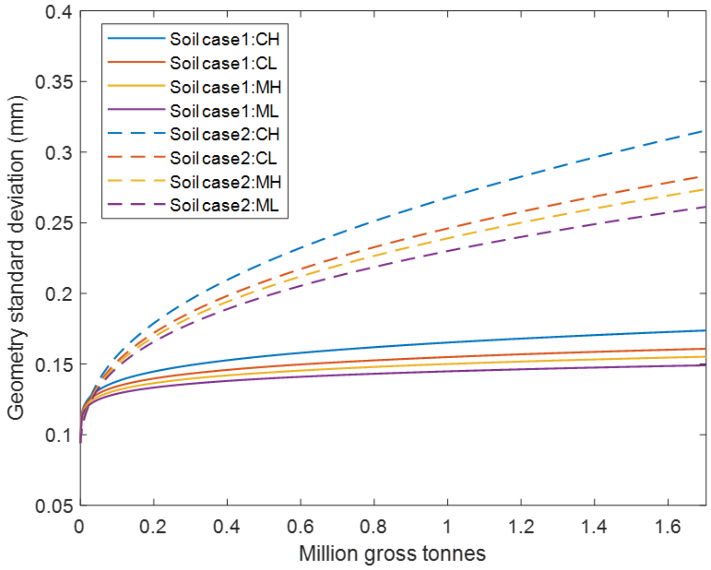

Figure 19. Track geometry evolution for varying subgrade properties

It is seen that both elastodynamic and settlement properties significantly influence on the evaluation of track geometry profile and deterioration. These properties are directly relevant to different soil types. However, there are still a number of influential variables that affect the track and the vehicle. Therefore, design charts can possibly be developed after performing more analyses.

7. Conclusions

Track geometry is an important parameter for scheduling track maintenance operations. Therefore this paper presents a novel numerical approach, capable of predicting track irregularity evolution for a wide range of situations. It has the following novel characteristics:

1. It's solved using a mixed frequency-wavenumber and time-space approach. This optimised solution procedure then allows for the track geometry profile to be updated after every load passage
2. The track and ground are fully coupled and modelled explicitly. This allows for 3D stress fields to be computed, which are important for accurate settlement calculation
3. The effect of strain on track and ground material properties is accounted for using an iterative equivalent linear approach
4. Modified settlement laws are used that can account for the differing forces induced due to evolving track profiles

Three aspects of the model are validated. These are its ability to accurately simulate track deflections and non-linearity, its ability to model train-track interaction, and its ability to predict future changes in vertical track profile. The validated model is then used to investigate the influence of updating the track geometry after each axle load on the differential settlement prediction. This confirms the importance of updating the track geometry profile as frequently as possible, particularly for softer soils. In addition, the effect of changing the elastodynamic and settlement properties of the subgrade are investigated. It is shown that stiffer soils give rise to markedly reduced settlement, thus highlighting the need for well-constructed track subgrade.

8. Acknowledgements

The authors are grateful to Network Rail for providing track geometry data, the University of Leeds, the Cheney fellowship scheme and the Leverhulme Trust UK (PLP-2016-270). They also acknowledge the financial support provided by the Spanish Ministries Science and Innovation and Universities under research project PID2019-109622RB-C21, and US-126491 funded by the FEDER Andalucía 2014-2020 Operational Program. Shift2Rail and IN2TRACK3 are also acknowledged.

Author contributions

C. Charoenwong: methodology, software, analysis, writing; D. P. Connolly: conceptualisation, methodology, resources, writing, supervision; P. Woodward: Reviewing; P. Galvin: supervision, writing; P. Alves Costa: supervision, writing

References

Abadi T, Le Pen L, Zervos A, Powrie W. A Review and Evaluation of Ballast Settlement Models using Results from the Southampton Railway Testing Facility (SRTF). Procedia Eng 2016;143:999–1006. https://doi.org/10.1016/j.proeng.2016.06.089.

Alves Costa P, Calçada R, Silva Cardoso A, Bodare A. Influence of soil non-linearity on the dynamic response of high-speed railway tracks. Soil Dyn Earthq Eng 2010;30:221–35. https://doi.org/10.1016/j.soildyn.2009.11.002.

Arcos R, Soares PJ, Alves Costa P, Godinho L. An experimental/numerical hybrid methodology for the prediction of railway-induced ground-borne vibration on buildings to be constructed close to existing railway infrastructures: Numerical validation and parametric study. Soil Dyn Earthq Eng 2021;150:106888. https://doi.org/10.1016/j.soildyn.2021.106888.

Bian X, Jiang H, Chang C, Hu J, Chen Y. Track and ground vibrations generated by high-speed train running on ballastless railway with excitation of vertical track irregularities. Soil Dyn Earthq Eng 2015;76:29–43. https://doi.org/10.1016/j.soildyn.2015.02.009.

Burrow MPN, Shi J, Wehbi M, Ghataora GS. Assessing the damaging effects of railway dynamic wheel loads on railway foundations. Transp Res Rec 2017;2607:62–73. https://doi.org/10.3141/2607-09.

Chen C, McDowell GR. An investigation of the dynamic behaviour of track transition zones using discrete element modelling. Proc Inst Mech Eng Part F J Rail Rapid Transit 2016;230:117–28. https://doi.org/10.1177/0954409714528892.

Colaço A, Costa PA, Connolly DP. The influence of train properties on railway ground vibrations. Struct Infrastruct Eng 2016;12:517–34. https://doi.org/10.1080/15732479.2015.1025291.

Connolly DP, Costa PA. Geodynamics of very high speed transport systems. Soil Dyn Earthq Eng 2020;130:105982. https://doi.org/10.1016/j.soildyn.2019.105982.

Connolly DP, Dong K, Alves Costa P, Soares P, Woodward PK. High speed railway ground dynamics: a multi-model analysis. Int J Rail Transp 2020;8:324–46. https://doi.org/10.1080/23248378.2020.1712267.

Cooley JW, Tukey JW. An Algorithm for the Machine Calculation of Complex Fourier Series Published by : American Mathematical Society Stable URL : https://www.jstor.org/stable/2003354 REFERENCES Linked references are available on JSTOR for this article : An Algorithm for the M 2019;19:297–301.

Costa PA, Calçada R, Cardoso AS. Influence of train dynamic modelling strategy on the prediction of track-ground vibrations induced by railway traffic. Proc Inst Mech Eng Part F J Rail Rapid Transit 2012;226:434–50. https://doi.org/10.1177/0954409711433686.

Dahlberg T. Some railroad settlement models - A critical review. Proc Inst Mech Eng Part F J Rail Rapid Transit 2001;215:289–300. https://doi.org/10.1243/0954409011531585.

Dong K, Connolly DP, Laghrouche O, Woodward PK, Alves Costa P. Non-linear soil behaviour on high speed rail lines. Comput Geotech 2019;112:302–18. https://doi.org/10.1016/j.compgeo.2019.03.028.

Dyvik R, Kaynia AM. Large-Scale Triaxial Tests on Railway Embankment Material. In: Stark T, Swan R, Szecsy R, editors. Railr. Ballast Test. Prop., West Conshohocken, PA: ASTM International; 2018, p. 173–90. https://doi.org/10.1520/STP160520170031.

Esveld C. Modern railway track. vol. 385. MRT-productions Zaltbommel; 2001.

Federal Railroad Administration. Statistical Representations of Track Geometry : Volume I. Washington, D.C.: 1980.

François S, Schevenels M, Galvín P, Lombaert G, Degrande G. A 2.5D coupled FE-BE methodology for the dynamic interaction between longitudinally invariant structures and a layered halfspace. Comput Methods Appl Mech Eng 2010. https://doi.org/10.1016/j.cma.2010.01.001.

Fröhling RD. Prediction of Spatially Varying Track Settlement. Conf Railw Eng CORE98 1998:103–9.

Grossoni I, Powrie W, Zervos A, Bezin Y, Le Pen L. Modelling railway ballasted track settlement in vehicle-track interaction analysis. Transp Geotech 2021;26:100433. https://doi.org/10.1016/j.trgeo.2020.100433.

Guo Y, Zhai W. Long-term prediction of track geometry degradation in high-speed vehicle–ballastless track system due to differential subgrade settlement. Soil Dyn Earthq Eng 2018;113:1–11. https://doi.org/10.1016/j.soildyn.2018.05.024.

Guo Y, Zhao C, Markine V, Jing G, Zhai W. Calibration for discrete element modelling of railway ballast: A review. Transp Geotech 2020;23:100341. https://doi.org/10.1016/j.trgeo.2020.100341.

Hardin BO, Drnevich VP. Shear modulus and damping in soils: design equations and curves. J Soil Mech Found Div 1972;98:667–92.

Hardy GH, Littlewood JE. An additional note on Parseval’s theorem. Math Zeitschrift n.d.;34.

Indraratna B, Nimbalkar S. Stress-Strain Degradation Response of Railway Ballast Stabilized with Geosynthetics. J Geotech Geoenvironmental Eng 2013;139:684–700. https://doi.org/10.1061/(asce)gt.1943-5606.0000758.

Indraratna B, Thakur PK, Vinod JS. Experimental and numerical study of railway ballast behavior under cyclic loading. Int J Geomech 2010;10:136–44.

Indraratna B, Thakur PK, Vinod JS, Salim W. Semiempirical Cyclic Densification Model for Ballast Incorporating Particle Breakage. Int J Geomech 2012;12:260–71. https://doi.org/10.1061/(asce)gm.1943-5622.0000135.

Ishibashi I, Zhang X. Unified dynamic shear moduli and damping ratio of sand and clay. Soils Found 1993;33:182–91.

Karlström A, Boström A. An analytical model for train-induced ground vibrations from railways. J Sound Vib 2006;292:221–41. https://doi.org/10.1016/j.jsv.2005.07.041.

Knothe K, Wu Y. Receptance behaviour of railway track and subgrade. Arch Appl Mech 1998;68:457–70. https://doi.org/10.1007/s004190050179.

Kouroussis G, Connolly DP, Verlinden O. Railway-induced ground vibrations – a review of vehicle effects. Int J Rail Transp 2014;2:69–110. https://doi.org/10.1080/23248378.2014.897791.

Lee JS, Hwang SH, Choi IY, Choi Y. Deterioration Prediction of Track Geometry Using Periodic Measurement Data and Incremental Support Vector Regression Model. J Transp Eng Part A Syst 2020;146:04019057. https://doi.org/10.1061/jtepbs.0000291.

Li D. Railway track granular layer thickness design based on subgrade performance under repeated loading. University of Massachusetts, Amherst, Mass, 1994.

Li D, Hyslip J, Sussmann T, Chrismer S. Railway geotechnics. CRC Press; 2015.

Li D, Selig ET. Cumulative Plastic Deformation for Fine-Grained Subgrade Soils. J Geotech Eng 1996;122:1006–13. https://doi.org/10.1061/(asce)0733-9410(1996)122:12(1006).

Li X, Ekh M, Nielsen JCO. Three-dimensional modelling of differential railway track settlement using a cycle domain constitutive model. Int J Numer Anal Methods Geomech 2016;40:1758–70.

Liu J, Xiao J. Experimental Study on the Stability of Railroad Silt Subgrade with Increasing Train Speed. J Geotech Geoenvironmental Eng 2010;136:833–41. https://doi.org/10.1061/(asce)gt.1943-5606.0000282.

Lopes P, Costa PA, Ferraz M, Calçada R, Cardoso AS. Numerical modeling of vibrations induced by railway traffic in tunnels: From the source to the nearby buildings. Soil Dyn Earthq Eng 2014;61–62:269–85. https://doi.org/10.1016/j.soildyn.2014.02.013.

Madshus C, Kaynia AM. High-speed railway lines on soft ground: dynamic behaviour at critical train speed. J Sound Vib 2000;231:689–701. https://doi.org/10.1006/jsvi.1999.2647.

Menan Hasnayn M, John McCarter W, Woodward PK, Connolly DP, Starrs G. Railway subgrade performance during flooding and the post-flooding (recovery) period. Transp Geotech 2017;11:57–68. https://doi.org/10.1016/j.trgeo.2017.02.002.

Network Rail. Track geometry - Inspections and minimum actions - NR/L2/TRK/001/mod11. London, UK: 2015.

Neuhold J, Landgraf M, Marschnig S, Veit P. Measurement Data-Driven Life-Cycle Management of Railway Track. Transp Res Rec 2020;2674:685–96. https://doi.org/10.1177/0361198120946007.

Nielsen JCO, Li X. Railway track geometry degradation due to differential settlement of ballast/subgrade – Numerical prediction by an iterative procedure. J Sound Vib 2018;412:441–56. https://doi.org/10.1016/j.jsv.2017.10.005.

ORE. Question D71: Stresses in the Rails, the Ballast and in the Formation Resulting from Traffic Loads. Stresses in the formation (results of the third phase ; measurements under dynamic conditions). International Union of Railways, Office for Research and Experiments; 1970.

Ramos A, Gomes Correia A, Indraratna B, Ngo T, Calçada R, Costa PA. Mechanistic-empirical permanent deformation models: Laboratory testing, modelling and ranking. Transp Geotech 2020;23. https://doi.org/10.1016/j.trgeo.2020.100326.

Rollins KM, Singh M, Roy J. Simplified Equations for Shear-Modulus Degradation and Damping of Gravels. J Geotech Geoenvironmental Eng 2020a;146:04020076. https://doi.org/10.1061/(asce)gt.1943-5606.0002300.

Rollins KM, Singh M, Roy J, AKKOÇ B. Simplified Equations for Shear-Modulus Degradation and Damping of Gravels. J Geotech Geoenvironmental Eng 2020b;146:04020076. https://doi.org/10.1061/(asce)gt.1943-5606.0002300.

Sato Y. Japanese Studies on Deterioration of Ballasted Track. Veh Syst Dyn 1995;24:197–208. https://doi.org/10.1080/00423119508969625.

Saussine G, Cholet C, Gautier PE, Dubois F, Bohatier C, Moreau JJ. Modelling ballast behaviour under dynamic loading. Part 1: A 2D polygonal discrete element method approach. Comput Methods Appl Mech Eng 2006;195:2841–59. https://doi.org/10.1016/j.cma.2005.07.006.

Sayeed MA, Shahin MA. Design of ballasted railway track foundations using numerical modelling. Part I: Development1. Can Geotech J 2018;55:353–68. https://doi.org/10.1139/cgj-2016-0633.

Shan Y, Zhou S, Zhou H, Wang B, Zhao Z, Shu Y, et al. Iterative method for predicting uneven settlement caused by high-speed train loads in transition-zone subgrade. Transp Res Rec 2017;2607:7–14. https://doi.org/10.3141/2607-02.

Sheng X, Jones CJC, Thompson DJ, Wu TX, Thompson DJ. A comparison of a theoretical model for quasi-statically and dynamically induced environmental vibration from trains with measurements. J Sound Vib 2003;267:621–35. https://doi.org/10.1016/S0022-460X(03)00728-4.

Shenton MJ. Ballast deformation and track deterioration. Track Technol 1985:253–65.

Shih JY, Grossoni I, Bezin Y. Settlement analysis using a generic ballasted track simulation package. Transp Geotech 2019;20:100249. https://doi.org/10.1016/j.trgeo.2019.100249.

Shih JY, Thompson DJ, Zervos A. The influence of soil nonlinear properties on the track/ground vibration induced by trains running on soft ground. Transp Geotech 2017;11:1–16. https://doi.org/10.1016/j.trgeo.2017.03.001.

Suiker ASJ, de Borst R. A numerical model for the cyclic deterioration of railway tracks. Int J Numer Methods Eng 2003;57:441–70. https://doi.org/10.1002/nme.683.

Thompson D. Railway noise and vibration: mechanisms, modelling and means of control. Elsevier; 2008.

Wu TX, Thompson DJ. Vibration analysis of railway track with multiple wheels on the rail. J Sound Vib 2001;239:69–97. https://doi.org/10.1006/jsvi.2000.3157.

Xu Q, Xiao Z, Liu T, Lou P, Song X. Comparison of 2D and 3D prediction models for environmental vibration induced by underground railway with two types of tracks. Comput Geotech 2015;68:169–83. https://doi.org/10.1016/j.compgeo.2015.04.011.

Yan TH, Corman F. Assessing and Extending Track Quality Index for Novel Measurement Techniques in Railway Systems. Transp Res Rec 2020;2674:24–36. https://doi.org/10.1177/0361198120923661.

Yu Z, Connolly DP, Woodward PK, Laghrouche O. Settlement behaviour of hybrid asphalt-ballast railway tracks. Constr Build Mater 2019;208:808–17. https://doi.org/10.1016/j.conbuildmat.2019.03.047.

Zhai W, Cai Z. Dynamic interaction between a lumped mass vehicle and a discretely supported continuous rail track. Comput Struct 1997;63:987–97.

https://doi.org/10.1016/S0045-7949(96)00401-4.

Zuada Coelho B, Varandas JN, Hijma MP, Zoeteman A. Towards network assessment of permanent railway track deformation. Transp Geotech 2021;29. https://doi.org/10.1016/j.trgeo.2021.100578.

Appendix. Vehicle mass and stiffness matrices

Mass and stiffness matrices of the vehicle system:

$$[Z] = \begin{bmatrix} 0 & 0 & 0 & 0 & 0 & 0 & 1 & 0 & 0 & 0 \\ 0 & 0 & 0 & 0 & 0 & 0 & 0 & 1 & 0 & 0 \\ 0 & 0 & 0 & 0 & 0 & 0 & 0 & 0 & 1 & 0 \\ 0 & 0 & 0 & 0 & 0 & 0 & 0 & 0 & 0 & 1 \end{bmatrix} \tag{50}$$

$$[M^v] = \begin{bmatrix} Mc & 0 & 0 & 0 & 0 & 0 & 0 & 0 & 0 & 0 \\ 0 & Jc & 0 & 0 & 0 & 0 & 0 & 0 & 0 & 0 \\ 0 & 0 & Mb & 0 & 0 & 0 & 0 & 0 & 0 & 0 \\ 0 & 0 & 0 & Jb & 0 & 0 & 0 & 0 & 0 & 0 \\ 0 & 0 & 0 & 0 & Mb & 0 & 0 & 0 & 0 & 0 \\ 0 & 0 & 0 & 0 & 0 & Jb & 0 & 0 & 0 & 0 \\ 0 & 0 & 0 & 0 & 0 & 0 & Mw & 0 & 0 & 0 \\ 0 & 0 & 0 & 0 & 0 & 0 & 0 & Mw & 0 & 0 \\ 0 & 0 & 0 & 0 & 0 & 0 & 0 & 0 & Mw & 0 \\ 0 & 0 & 0 & 0 & 0 & 0 & 0 & 0 & 0 & Mw \end{bmatrix} \tag{51}$$

$$[K^v] = \begin{bmatrix} 2Ks & 0 & -Ks & 0 & -Ks & 0 & 0 & 0 & 0 & 0 \\ 0 & 2Ks \cdot lb^2 & -Ks \cdot lb & 0 & Ks \cdot lb & 0 & 0 & 0 & 0 & 0 \\ -Ks & -Ks \cdot lb & Ks + 2Kp & 0 & 0 & 0 & -Kp & -Kp & 0 & 0 \\ 0 & 0 & 0 & 2Kp \cdot lw^2 & 0 & 0 & -Kp \cdot lw & Kp \cdot lw & 0 & 0 \\ -Ks & Ks \cdot lb & 0 & 0 & Ks + 2Kp & 0 & 0 & 0 & -Kp & -Kp \\ 0 & 0 & 0 & 0 & 0 & 2Kp \cdot lw^2 & 0 & 0 & -Kp \cdot lw & Kp \cdot lw \\ 0 & 0 & -Kp & -Kp \cdot lw & 0 & 0 & Kp & 0 & 0 & 0 \\ 0 & 0 & -Kp & Kp \cdot lw & 0 & 0 & 0 & Kp & 0 & 0 \\ 0 & 0 & 0 & 0 & -Kp & -Kp \cdot lw & 0 & 0 & Kp & 0 \\ 0 & 0 & 0 & 0 & -Kp & Kp \cdot lw & 0 & 0 & 0 & Kp \end{bmatrix} \tag{52}$$

where Mc is mass of the car box; Mb is mass of the bogie; Mw is mass of the wheelset; Jb is the rotation inertia of the car body; Kp is the complex stiffness of the primary suspension; Ks is the complex stiffness of the secondary suspension; lb is half the distance between the bogie's centre of gravity; and lw is half the wheelbase that shares the same bogie. Kp and Ks are defined as:

$$Kp = k_{pri} + i\omega c_{pri} \tag{53}$$

$$Ks = k_{sec} + i\omega c_{sec} \tag{54}$$

where k_{pri} is the spring stiffness of the primary suspension; k_{sec} is the spring stiffness of the secondary suspension; c_{pri} is the viscous damping of the primary suspension; and k_{sec} is the viscous damping of the secondary suspension.